Structure–function relationship in an archaebacterial methionine sulfoxide reductase B

Michela Carella[1], Juliane Becher[1], Oliver Ohlenschläger[1], Ramadurai Ramachandran[1], Karl-Heinz Gührs[1], Gerd Wellenreuther[2], Wolfram Meyer-Klaucke[2], Stefan H. Heinemann[3] and Matthias Görlach[1*]

[1]Leibniz-Institut für Altersforschung/Fritz-Lipmann-Institut, Beutenbergstr. 11, D-07745 Jena, Germany

[2]EMBL Hamburg/DESY, Notkestr. 85, D-22603 Hamburg, Germany

[3]Zentrum für Molekulare Biomedizin, Institut für Biochemie und Biophysik, Friedrich-Schiller-Universität, Hans-Knöll-Str. 2, D-07745 Jena, Germany

Running title: Structure–function relationship in an archaeal MSRB

Keywords: Reactive oxygen species; Oxidative stress; NMR spectroscopy; Methionine sulfoxide reductase; Thioredoxin; Archaea.

Correspondence:

email: mago@fli-leibniz.de; tel.: +49-3641-656220; fax: +49-3641-656225.

Summary

Oxidation of methionine to methionine sulfoxide (MetSO) may lead to loss of molecular integrity and function. This oxidation can be 'repaired' by methionine sulfoxide reductases (MSRs), which reduce MetSO back to methionine. Two structurally unrelated classes of MSRs, MSRA and MSRB, show stereoselectivity towards the S and the R enantiomer of the sulfoxide, respectively. Interestingly, these enzymes were even maintained throughout evolution in anaerobic organisms.

Here, the activity and the NMR structure of MTH711, a zinc containing MSRB from the thermophilic, methanogenic archaebacterium *Methanothermobacter thermoautotrophicus* is described. The structure appears more rigid as compared to similar MSRBs from aerobic and mesophilic organisms. No significant structural differences between the oxidised and the reduced MTH711 state can be deduced from our NMR data. A stable sulfenic acid is formed at the catalytic Cys residue upon oxidation of the enzyme with MetSO. The two non–zinc–binding cysteines outside the catalytic centre are not necessary for activity of MTH711 and are not situated close enough to the active site cysteine to serve in regenerating the active centre via the formation of an *intra*molecular disulfide bond. These findings imply a reaction cycle that differs from that observed for other MSRBs.

Introduction

Reactive oxygen species (ROS) encompass a variety of chemical species formed by single electron transfers onto oxygen and are involved in various physiological and pathophysiological processes (D'Autreaux & Toledano, 2007, Finkel, 2003, Giorgio *et al.*, 2007). ROS can cause various forms of irreversible and reversible oxidative modification of proteins (Berlett & Stadtman, 1997, Halliwell & Gutteridge, 1999, Johnson & Travis, 1979, Stadtman & Berlett, 1997), lipids (Halliwell & Gutteridge, 1999) and DNA (Beckman & Ames, 1998) that eventually may cause loss of molecular function.

Oxidative damage of proteins is considered to be a significant contributor to molecular ageing and age-related disease (Giorgio et al., 2007, Sohal, 2002) and several mechanisms have evolved to prevent or reverse these damages. Methionine (Met) is among the amino acids most susceptible to oxidation by almost all forms of ROS (D'Autreaux & Toledano, 2007, Giorgio et al., 2007, Glaser *et al.*, 1992, Stadtman *et al.*, 2005, Vogt, 1995). Met oxidation to MetSO can be reversed by methionine sulfoxide reductases (MSRs) (Hoshi & Heinemann, 2001). Evidence has accumulated suggesting that Met oxidation plays an important role in the development and progression of neurodegenerative disorders like Alzheimer´s (Schoneich, 2005) and Parkinson´s disease (Glaser *et al.*, 2005, Wassef *et al.*, 2007). However, surface-exposed Met in proteins (such as in glutamine synthetase) could also serve as antioxidants via cyclic oxidation and reduction (Levine *et al.*, 1996) and selective oxidation of critical Met within selected proteins permits their use as sensors of oxidative stress (Bigelow & Squier, 2005). Indeed, Met oxidation induces a conformational switch that modulates the activity of central regulatory proteins, *e.g.* Ca-ATPase, CaMKII, phospholamban and calmodulin (CaM) (Bigelow & Squier, 2005, Erickson *et al.*, 2008). These conformational switches are directly coupled to cellular redox conditions through the action of methionine sulfoxide reductases and function as a rheostat of cellular metabolism to

maintain optimal cell function with minimal levels of non specific oxidative damage to other biomolecules (Bigelow & Squier, 2005).

By their action, the MSR enzymes may regulate protein function, may be involved in signal transduction pathways, and may prevent cellular accumulation of faulty proteins (Bigelow & Squier, 2005, Hoshi & Heinemann, 2001, Moskovitz, 2005). Malfunction of the MSR system can lead to cellular changes resulting in compromised antioxidant defense, enhanced age-associated diseases involving neurodegeneration and modulation of life-span (Moskovitz, 2005, Petropoulos & Friguet, 2006, Shchedrina *et al.*, 2009, Wong *et al.*, 2010). Methionine oxidation results in the formation of the two diastereomers methionine-*S*-sulfoxide (Met-(S)-SO) and methionine-*R*-sulfoxide (Met-(R)-SO), which are reduced by either MSRA (Met-(S)-SO) or MSRB (Met-(R)-SO), respectively (Stadtman *et al.*, 2003). These two classes of enzymes display neither sequence nor structural homology, but share a 'mirrored catalytic mechanism' (Boschi-Muller *et al.*, 2005, Lowther *et al.*, 2002). Hence, this represents an compelling case of convergent evolution. Alignment of MSRB sequences reveals only a single Cys that is conserved in all family members (Fig. 1). This Cys is located in the C-terminal part of the protein and is the catalytic residue that directly attacks methionine sulfoxide (Kumar *et al.*, 2002). The first step in the catalytic cycle (reductase step) leads to the formation of a sulfenic acid intermediate on the catalytic Cys with the concomitant release of reduced Met. Immediately, an *intra*molecular disulfide bond is formed via the attack of a second Cys (recycling Cys) on the sulfenic acid intermediate and the release of a water molecule. Finally, this disulfide bond is reduced via an *inter*molecular thiol-disulfide exchange by thioredoxin (Boschi-Muller *et al.*, 2000, Lowther et al., 2002, Olry *et al.*, 2002) to regenerate the active site Cys-thiol function. The second Cys that is involved in the recycling of the active site ("recycling Cys") is not universally conserved (Fig. 1) (Kumar et al., 2002, Lowther et al., 2002, Neiers *et al.*, 2004, Ranaivoson *et al.*, 2009,

Tarrago *et al.*, 2009). Recent functional and structural analyses of MSRB enzymes indicate that the recycling Cys may be located farther away from the active centre necessitating structural rearrangement during the recycling process to allow for *intra*molecular disulfide-bond formation (Neiers et al., 2004, Ranaivoson et al., 2009). Many MSRB sequences carry four additional conserved Cys residues that are organised in two CXXC motifs (Fig. 1), which co-ordinate a zinc ion required for the enzymatic activity in the *E. coli* and *Drosophila* MSRB (Kumar et al., 2002, Olry *et al.*, 2005).

Despite the fact, that MSRs appear to have evolved as a molecular answer to environmental oxygen they are also found in strictly anaerobic prokaryotes including methanogenic thermophilic archea, *e.g. Methanothermobacter thermoautotrophicus* (Delaye *et al.*, 2007). This organism encodes a Zn-binding MSRB and we refer to it as MTH711 (Entrez Gene database; GeneID 1470672). MTH711 lacks a Cys in the semiconserved "recycling position" but still carries two extra Cys in addition to the Zn-binding ones. In order to elucidate the structural basis of catalytic centre recycling in this enzyme we solved the nuclear magnetic resonance (NMR)-based solution structure of MTH711 in its oxidised form because we consider this form particularly informative with respect to the recycling intermediate. Based on the structural and biochemical results presented here, the role of the bound zinc as well as the regeneration of the active site cysteine during the catalytic cycle is evaluated with respect to previous structural and enzymatic studies of MSR enzymes.

Results

Enzymatic activity

The stereospecific MSR activity of MTH711 was assessed in the presence of DTT using as substrates the free oxidised amino acids Met-(R)-SO and Met-(S)-SO, which are typically reduced by MSRB- or MSRA-type enzymes, respectively. MTH711 reduced Met-(R)-SO and was inactive for Met-(S)-SO (Fig. 2A), showing that it is an MSR of type B. The MSRB activity of MTH711 in the presence of either DTT or thioredoxin (Trx) as electron donors was further addressed using as substrate the synthetic peptide KIFM(O)K. As this peptide contains a racemic mixture of Met-(S/R)-SO, a reduction of only ~50% of the substrate is expected for the MSR type B MTH711. Full reduction of the peptide can only be achieved by a combination of MTH711 with a type A MSR (see below). The enzymatic activity assay showed that MTH711 has MSRB activity and uses DTT as well as cysteine as electron donor *in vitro* (Fig. 2G, J). In addition, a mutant MTH711 containing only the active site Cys139 but carrying Cys-to-Ser mutations in positions 69 and 112 was also active in the presence of both, free cysteine and DTT (Fig. 2K, L). Although MTH711 was active in the presence of DTT, it exhibited no activity in the presence of the archaeal thioredoxin homologues NHO (Genentrez: MTH807, GeneID 1471215) and ILO (Genentrez: MTH895, GeneID 1471303) (Amegbey *et al.*, 2003, Bhattacharyya *et al.*, 2002), respectively (Fig. 2M). Furthermore, neither human nor *E. coli* Trx elicited significant activity of MTH711 (Fig. 2O). In control experiments with human MSRA activity was detected in the presence of DTT and NHO (Fig. 2H, N) as well as with human and *E. coli* Trx (Fig. 2P). Finally, MTH711 and hMSRA together completely reduced the oxidised peptide in the presence of DTT (Fig. 2I). Reduction of the oxidised peptide was not detected in the presence of only DTT (Fig. 2C) or of MTH711 and/or MSRA in the absence of DTT (Fig. 2D, E, F). In addition, taking advantage of changes in electrophoretic mobility in SDS-gel of CaM following methionine

oxidation (Bartlett *et al.*, 2003), the ability of MTH711 to reduce CaM_{ox} in the presence of DTT was also addressed (Fig. S1). MTH711 partially reduced H_2O_2-oxidised calmodulin in the presence of DTT. Consistent with the results obtained for the oxidised peptide shown above, the DTT-dependent reduction of CaM_{ox} back to CaM was complete in the presence of both, MTH711 and hMSRA (Fig. S1).

Oxidation of the catalytic Cys139 in MTH711

For the NMR analysis, MTH711 from *Methanothermobacter thermautotrophicus* was produced in uniformly [^{15}N]- or [^{15}N, ^{13}C]-labelled form by recombinant expression and purified under non-denaturing conditions. Initial analysis of [^{1}H,^{15}N]-HSQC spectra revealed the presence of two signals for a subset of resonances of freshly prepared protein (not shown). Further experimentation indicated that this was due to the presence of two states of MTH711. Complete interconversion between the two states was achieved by addition of high (100 mM) concentrations of the reductant DTT (Fig. 3A, blue contours) or of the (oxidising) substrate MetSO (20 mM; Fig. 3A, red contours). In the absence of DTT or MetSO, MTH711 was converted within 1–2 days, most likely by atmospheric oxygen, into a form (Fig. 3B) identical to the one observed in the presence of excess MetSO (Fig. 3A, red contours). We concluded that this represents the oxidised state of the enzyme, which was also assessed by MALDI-TOF mass spectrometry. Two species, *i.e.* one major and one minor peak, were observed for both the reduced and the oxidised form (Table 1). The calculated and the observed mass for the major peak corresponds to MTH711 devoid of the zinc ion. The calculated and the observed mass for the minor peak is consistent with MTH711 still in complex with zinc. Hence, it appears that the co–ordinated zinc ion (see also EXAFS analysis below) is not lost completely upon desorption from the matrix into the gas phase during analysis. Incidentally, removal of zinc from MTH711 in solution by EDTA was not possible (data not shown).

Importantly, the mass difference between reduced and oxidised MTH711 species amounts to 16 Da (major peaks, Table 1) or 14 Da (minor peaks, Table 1). This is consistent with the formation of a sulfenic acid on the active site Cys139 upon oxidation of MTH711 by MetSO. The presence of a sulfenic acid on the active site Cys139 in the oxidised enzyme was confirmed by using the TNB assay (Fig. 4). For the wild type enzyme we find that in the presence of saturating concentrations of MetSO 0.93 moles of oxidised TNB^- per mole of MTH are formed. For the double mutant (C69S/C112S), which retaines only the active site Cys, 0.84 moles of oxidised TNB^- are formed in the same assay and no TNB^- oxidation was observed for the active site C139S mutant. These results clearly demonstrate the formation of a stable sulfenic acid moiety on the catalytic Cys after incubation with the substrate MetSO. The reaction is completely reversible after addition of DTT (Fig. 4) indicating complete release of the TNB moiety from the MTH–TNB adduct formed during the first phase of the assay.

Structure determination

The oxidised form of MTH711 turned out to exhibit sufficient longterm stability at 45 °C for a full NMR analysis of this thermophile-derived protein. At lower temperatures, the quality of spectra deteriorated. The well-dispersed signals of the [^{1}H,^{15}N]-HSQC spectrum of oxidised MTH711 (Fig. 3B) indicated a folded protein. The resonance assignments for MTH711 were derived from standard triple resonance experiments as described elsewhere (Carella *et al.*, 2010). An almost complete set of ^{1}H, ^{15}N, and ^{13}C assignments was achieved with the exception for residues Gly1-Met4, which represent the non-native residues derived from the vector sequence, Pro50-Phe52, Lys55-His60, Ser83 and Pro131-Arg132, and included all asparagine and glutamine side-chain NH_2 groups. In addition, assignment of the backbone amide groups under reducing conditions was obtained.

The MTH711 structure was calculated on the basis of 2428 NOE constraints and 388 torsion angle constraints. The $^{13}C^{\alpha}$ and $^{13}C^{\beta}$ chemical shifts indicated (Kornhaber *et al.*, 2006) that the Zn^{2+} ion is coordinated by cysteine residues 67, 70, 116 and 119. EXAFS analysis revealed that one zinc ion is co-ordinated by those four cysteines with a Zn-S distance of 2.33 Å each (Fig. 5; Table 2). This geometry, typical for a structural zinc-binding site (Auld, 2001), was utilised during the final structure calculations by including appropriate distance constraints. Amide hydrogen bonds forming consistently during initial structure calculations were included as additional constraints into the final structure calculation. For the β-sheets and helix α2, these hydrogen bonds correspond to amide protons for which an intermediate or slow exchange was observed in $^{1}H/^{2}H$ exchange experiments (data not shown). The resulting structure ensemble representing a well-defined solution structure was subjected to energy minimisation. The 20 energy minimised structures with the lowest DYANA target function are shown in Fig. 6A. The overall r.m.s.d. of this ensemble amounts to 0.8 Å for all backbone atoms excluding the unassignable residues. Table 2 summarises the experimental restraints used in structure calculations, restraint violations and structure statistics for the final set of the 20 energy minimised structures.

Solution structure

The solution structure of MTH711 from *Methanothermobacter thermautotrophicus* adopts a β1-β2-α1-α2-β3-β4-β5-β6-β7-β8-β9-β10 topology (Fig. 6B). All β-strands arrange in an anti-parallel manner: strands β1 (Ile8-Ser12), β2 (Arg17-Val21) form an extended and separated sheet at the N-terminus; strands β3 (Ile64-Ile68), β4 (Thr72-Asp76), β5 (Pro88-Tyr91), β6 (Lys136-Asn141) and β10 (Ala143-Pro149) enclose a core of hydrophobic aromatic side-chains and together with β7 (Val110-Leu115), β8 (Leu123-Asp128) and β9 (Ala143-Pro149) form an eight-stranded β-barrel like structure, as also indicated by low

hydrogen exchange and the high number of NOEs for the H^N and the H^α between the strands. The central β-sheet is flanked on one side by the two short α1- and α2-helices (Asp29-Arg32 and Ala39-Lys45, respectively) both of which are anchored to the core by hydrophobic amino acid residues.

The β-strands β3-β10 constitute the best-defined regions of the protein structure (backbone r.m.s.d. 0.32 Å; see also Fig. 6A) as also reflected by a high density of long-range NOE contacts. Apart from the region Pro50-His60 harbouring the unassigned residues, the loop connecting the strands β4-β5 (Phe81-Trp87) is the least well defined of the connecting structural elements (backbone r.m.s.d. 0.9 Å); this conserved loop is primarily defined by intra-residue NOE-derived restraints. Most of the hydrogen-bonded amide protons of the β-sheets remain unexchanged in deuterated solvent even beyond 12 hours (data not shown), providing evidence that they constitute stable and rigid structural elements. However, a difference can be seen for the two helices: helix α2 is more stable, as indicated by the slow $^1H/^2H$ exchange and shows 17 NOE contacts to strands β3 and β10. Helix α1, instead, shows only 8 interresidual NOE contacts and a faster amide proton $^1H/^2H$ exchange (data not shown) indicating it to be less stable.

The S^2 order parameters (Fig. 7) as derived by model-free analysis (Lipari & Szabo, 1981) of [^{1}H]-^{15}N heteronuclear NOEs and T_1 and T_2 relaxation data indicate that a large proportion of the MTH711 backbone is essentially rigid on the ps to ns time scale. S^2 values below 0.8 were observed for residues Asp61 immediately following the unassigned stretch Pro50-His60 as well as for Arg7, Arg23, Glu25, Ser106, Met109, Val110, Asp128 and Thr134 all of which are located in loop regions. No significantly increased dynamics is observed for any of the Cys residues (Fig. 6D) or residues in and around the catalytic centre (Fig. 6C). These observations are consistent with an overall well ordered structure undergoing

isotropic tumbling with a τ_c of 6.3 nsec. This rotational correlation time is compatible with a monomeric 15 kDa protein.

Zinc co–ordination and active site

The CXXC motifs co-ordinating the zinc ion are located in the turns connecting the strands β3-β4 (Cys67-Cys70) and β7-β8 (Cys116-Cys119), respectively. The zinc-binding site and the active site (catalytic Cys139) are clearly separated by more than 15 Å (Fig. 6B).

The catalytic Cys (Fig. 6B, C, D) is located within strand β8 and the side-chain points towards the solvent from the bottom of a surface-exposed active site. Most of the residues surrounding the catalytic Cys are found in conserved regions of MSRB sequences (Fig. 1; Fig. 6C) and are involved in the catalytic mechanism (Boschi-Muller et al., 2005, Kumar et al., 2002, Lowther et al., 2002). However, close to the catalytic Cys there is no second cysteine (Fig. 6C) necessary for the formation of an *intra*molecular disulfide bridge during the regeneration of the active site as observed for other MSRs (Boschi-Muller et al., 2005, Coudevylle *et al.*, 2007, Kumar et al., 2002, Lowther et al., 2002, Ranaivoson et al., 2009). Rather, the two remaining free Cys residues (Cys69 and Cys112) are located 14 or 15 Å away from the catalytic site (Fig. 6D) and their substitution (C69S/C112S) does not affect the activity of MTH (Fig. 2K, L) indicating that formation of an *intra*molecular disulfide bridge is not essential for the reaction mechanism in MTH. In agreement with this, for both the wild type and the double mutant enzyme, the difference of thiol content observed between the reduced and the oxidised state of the enzyme amounts to one thiol group as determined by the DTNB assay (data not shown).

Discussion

Given the importance of balancing oxidative protein modifications for cell functions and long-term survival there is the need of understanding the molecular details by which methionine sulfoxide reductases 'repair' proteins by reducing methionine sulfoxide back to methionine. Since little is known about the role and molecular function of MSRBs in anaerobic organisms, we carried out the NMR structural analysis of oxidised MTH711, a methionine sulfoxide reductase of type B, from the thermophilic methanogenic archaebacterium *M. thermoautotrophicus*. MTH711 is highly homologous to other MSRBs, including the human enzymes (Fig. 1). The MSR activity, including recycling, of MTH711 as well as its substrate specificity were assessed. MTH711 reduces both free and protein-bound MetSO and is specific for the R-form of Met-(R)-SO enantiomer (Fig. 2; Supporting Fig. 1). However, efficient recycling of the enzyme *in vitro* could only be achieved by DTT and free cysteine but not by Trx or Trx homologues from *M. thermoautotrophicus* (Fig. 2).

The three dimensional solution structure of oxidised MTH711 (Fig. 6) was determined by heteronuclear NMR spectroscopy. Excluding the region, which could not be assigned and, hence, appears disordered, the structure is well defined (Fig. 6A; Table 2) and confirms the unrelatedness of the folds of MSRBs and MSRAs (*E. coli* pdb 1FF3; *B. taurus* pdb 1FVA and 1FVG; *M. tubercolosis* pdb 1NWA; *N. meningiditis* pdb 3BQE; *N. gonorrhoeae* pdb 2H30). MTH711 adopts mainly a barrel-like topology, similar to that reported for MSRBs from the mesophilic bacteria *Neisseria gonorrhoeae* (pdb 1L1D), *Bacillus subtilis* (pdb 1XM0), *Xanthomonas campestris* (pdb 3HCI) and *Burkholderia pseudomallei* (pdb 3C3Z). Like MTH711, the *Burkholderia pseudomallei* and *Xanthomonas campestris* MSRB are also zinc-containing enzymes. The lack of the two N-terminal β-strands both in the *Burkholderia pseudomallei* and *Xanthomonas campestris* crystal structure but present in MTH711 accounts for the main overall structural difference between the proteins. Comparison of the structures

(not shown) reveals that the common β-strands superimpose with an r.m.s.d. of 2.3 Å for *Burkholderia pseudomallei* and 1.9 Å for *Xanthomonas campestris*. The presence of the zinc ion, however, does not significantly change the structure of MTH711 as compared to the Zn-free *Neisseria gonorrhoeae* PilB MSRB domain (Fig. 8).

At least 50% of the available MSRB sequences possess four cysteines residing in two CXXC motifs (Boschi-Muller et al., 2005), which generate a Zn^{2+}-binding site that in MTH711 is located at positions Cys67-Cys70 and Cys116-Cys119 (highlighted in blue in Fig. 1). The zinc ion appears to be firmly bound as attempts to remove it by dialysing MTH711 against EDTA failed to extract significant amounts of the metal (data not shown) despite its accessible position on the protein surface (Fig. 6B). Consistent with this, we also observed incomplete removal of the zinc ion during MALDI–TOF analysis (Table 1). Studies on the *D. melanogaster* and the *E. coli* MSRB, which also carry this Zn^{2+}-binding site, showed that substituting the four Cys residues of the metal-binding site results in complete loss of metal and of catalytic activity (Kumar et al., 2002, Olry et al., 2005). Substitution of the four Cys residues in *E. coli* MSRB also induces a loss of secondary structure content and of thermostability (Olry et al., 2005). The MSRB enzymes that do not possess the metal-binding site carry at the corresponding positions the conserved residues Asp, Ser and Ala (highlighted in grey in Fig. 1), which are not conducive to providing stabilising interactions to a zinc ion. Insertion of four cysteine residues into these positions results in the tight binding of one zinc ion, in no significant change of the local conformation of the enzyme and in increased thermal stability (Boschi-Muller et al., 2005). From this it appears that the zinc–binding capability carries an important structure stabilising role in thermophilic organisms, which may well be dispensable in mesophilic organisms (*N. gonorrhoeae, B. subtilis)*. The observation that there are zinc-binding MSRBs, including the human ones (Hansel *et al.*, 2005), in mesophilic organisms is puzzling in this context. However, it supports the notion

(Kumar et al., 2002), that the zinc-containing MSRBs are the prototypical enzymes, some descendants of which have lost zinc–binding capability later in evolution.

The MTH711 structure is indicative of the zinc ion not being involved in catalysis as concluded from the location of the metal binding site 15 Å away from the active site (Fig. 6B). This conclusion is further supported by the observation that structural zinc sites contain four protein ligands (mostly Cys, as observed here) and no bound water molecule. In contrast, in catalytic sites the zinc generally forms complexes with water and any three nitrogen, oxygen and sulfur donors with His being the predominant amino acid (Auld, 2001). Even though not yet characterised in detail, the first step of the catalytic mechanism of MTH711 is very likely to be similar to that already described for other MSRs (Olry et al., 2002) as judged from the active site structure (Fig. 6C). This MetSO reducing step consists of a nucleophilic attack by the catalytic Cys139 onto the substrate, which is followed by the rearrangement of the resulting intermediate leading to the formation of a sulfenic acid on the catalytic Cys139. The regeneration of the thiol function of the catalytic Cys139 through an *intra*molecular disulfide is dependent upon the presence of a "recycling" Cys. This disulfide is subsequently resolved by an external reductant such as DTT (*in vitro*) or thioredoxin (*in vivo*) (Lowther et al., 2002, Weissbach *et al.*, 2002). However, no such recycling Cys is present in MTH711 where Thr85 occupies the corresponding position, which is located in the loop connecting strand β4-β5. Hence, the 'canonical' recycling mechanism outlined above is not expected for MTH711. One possibility would be a conformational rearrangement allowing for an approach of a Cys located in a non-conserved remote position during the catalytic cycle similar to the situation in MSRA of *E. coli* (Coudevylle et al., 2007) and MSRB from *X. campestris* (Ranaivoson et al., 2009) where such a rearrangement is observed between the reduced and the oxidised forms. However, the region in *X. campestris* (His24-Asp40), which rearranges to form the disulfide bond there (Ranaivoson et al., 2009), corresponds to residues Ala45 to

Asp58 not carrying a Cys residue in MTH711. Both candidate cysteine thiol functions here (Cys69 and Cys112) are clearly too far away (~ 15Å; Fig. 6D) in the oxidised MTH711 to form a disulfide bridge with the catalytic cysteine (Cys139). Furthermore, only minor differences between the oxidised and the reduced state can be observed. Addition of 100 mM DTT to oxidised MTH711 yields a perturbation of chemical shifts (Fig. 3A, Fig. 9A). The amide groups of residues around the active site (but not the catalytic Cys139) as well as Cys112 and its neighbours (Fig. 9B) but not Cys69, which is embedded in the first CXXC motif ($CIC_{69}C$), experience a perturbation of more than 0.1 ppm (Fig. 9A). However, the rather limited magnitude of the chemical shift perturbation may well arise from a combined effect of smaller local rearrangements and of the oxidation of the active site. Hence, Cys69 and Cys112 are not subject to major structural rearrangements, equivalent to the ones observed for *X. campestris* MSRB and *E. coli* MSRA (Coudevylle et al., 2007, Ranaivoson et al., 2009). Moreover, the C69S/C112S MTH double mutant is enzymatically active (Fig. 2K, L) and a stable sulfenic acid is observed in the oxidised enzyme (Fig. 4, Table 1). Taken together, our structural and biochemical data show that recycling of MTH711 is not dependent upon an *intra*molecular disulfide involving Cys69 and Cys112. Therefore, a different recycling mechanism with respect to the one described for the other MSRs (Boschi-Muller et al., 2005) is very likely to be operational in MTH711 and MSRBs with similar properties. In this context we note, that MSRBs of *Rhodobacter capsulatus* and *Arabidopsis thaliana* do not contain other cysteine residues outside the active centre and the zinc-binding CXXC motives (Neiers et al., 2004, Tarrago et al., 2009), necessitating a recycling mechanism without *intra*molecular disulfide bond formation.

Interestingly, up to now no other wild type MSR structure containing a stable cysteine sulfenic acid moiety has been reported. Usually, Cys-SOH represents a transient intermediate but for several enzymes stable Cys-SOH have been described (reviewed in (Claiborne *et al.*,

1993, Kettenhofen & Wood, 2010, Poole *et al.*, 2004)). Evidence for stable Cys-SOH were reported for MSRA and MSRB mutants where disulfide forming Cys residues were replaced by Ser (Boschi-Muller et al., 2000, Neiers et al., 2004, Olry et al., 2002, Ranaivoson *et al.*, 2008). Three factors could in principle contribute to the observed stability of the SOH intermediate in MTH711: an apolar environment, the lack of a vicinal thiol, which would form a disulfide, or the formation of a hydrogen bond (Claiborne et al., 1993). The active site Cys side chain is solvent exposed and not located in a particularly apolar environment but the hydrophobic Trp87 side chain as well as the three methylene groups of the Arg137 side chain (Fig. 6C) could potentially contribute to such a stabilisation of the SOH. As discussed above, in the structure of the oxidised, Cys-SOH containing MTH711 there is no vicinal Cys available for the formation of a disulfide and the observation of a stable SOH is fully consistent with this. Finally, for His125 a backbone amide chemical shift perturbation significantly larger than for all other residues is observed between the reduced and the oxidised state of the enzyme (Fig. 9A). A rearrangement of the His125 side chain during the MetSO reducing step of the catalytic cycle resulting in the formation of the SOH (Boschi-Muller *et al.*, 2008) at the catalytic Cys139 may cause such a chemical shift perturbation through local conformational and ring current effects. One could speculate that such a reoriented His125 side chain engages in hydrogen bonding with the SOH moiety, thereby contributing to its stability. However, this hydrogen bonding would have to be water–mediated due to the average distance of 6.3 Å observed between the S^{γ} of Cys139 and the N^{δ} of the His125 in the calculated MTH711 structures.

In order to restore the catalytically competent Cys139 thiol function, the sulfenic acid formed on the catalytic cysteine could be directly reduced during the recycling step by a thioredoxin (Kim & Gladyshev, 2004, Tarrago *et al.*, 2010) or by another (unknown) reducing enzyme. Therefore, we recombinantly expressed, purified and tested the two Trx homologues

ILO and NHO from *M. thermoautotrophicus* (Amegbey et al., 2003, Bhattacharyya et al., 2002) for activity. Even though NHO exhibited recycling activity towards human MSRA at 37 °C, neither of the two promoted MTH711 recycling (Fig. 2M). In addition, we did not detect activity of MTH711 in the presence of human or *E. coli* Trx, both of which are sufficient to drive human MSRA activity (Fig. 2O, P), suggesting that species specificity is not an issue here. As glutathione is to the best of our knowledge not present in this methanogenic archaeon (see also (Amegbey et al., 2003, Bhattacharyya et al., 2002)), we tried to identify other potential physiological low molecular weight recycling agents for MTH711. Here we found, that free cysteine works with wild–type and mutant MTH711 *in vitro* (Fig. 2J, K). We also tested coenzyme M (CoM, 2-mercaptoethanesulfonic acid), which is very abundant in *M. thermoautotrophicus* and required for methyl transfer reactions in methanogens (Balch & Wolfe, 1979, Fahey, 2001). CoM, even under a protective argon atmosphere, did not promote MTH711 activity *in vitro* at 30 mM (data not shown), which is 15-fold the physiological concentration (Balch & Wolfe, 1979). Also no MTH711 activity was observed in the presence of either ILO or NHO in combination with CoM (data not shown). The finding that MTH711 is not recycleable directly by *M. thermoautotrophicus* thioredoxin homologues and one potential physiological SH donor (CoM) *in vitro,* does not exclude their recycling activity *in vivo*. Taking into account that free cysteine supports recycling of the active centre (Fig. 2J, K) and a strongly reducing intracellular environment in methanogenic organisms (Thauer *et al.*, 2008), a recycling mechanism involving virtually any thiol containing moiety with an appropriate redox potential (Jacob *et al.*, 2003, Sagher *et al.*, 2006) could be operational *in vivo.* Such a thiol could dissolve a mixed MTH711–Cys disulfide recycling intermediate thereby re–generating the active site Cys thiol function .

As *M. thermoautotrophicus* grows under strictly anaerobic conditions (Smith *et al.*, 1997), the evolutionary conservation of both MSRA and MSRB in this organism is not

necessarily expected but may be explained by their protective role to respond to metabolically generated ROS or following transient and low level exposure to exogeneous oxygen (Delaye et al., 2007). The latter situation would be expected at temperatures below the optimal thriving condition (65 °C), where solubility of oxygen in the media is increased. Incidentally, for the hyperthermophilic archeon *T. kodakaraensis* a significantly increased expression of an MSRAB enzyme was reported at reduced growth temperatures (Fukushima *et al.*, 2007). Hence, we dare to speculate that in such organisms efficient recycling of MSRs by a specific system might not even be essential under optimal growth conditions and that it might suffice to rely upon the pool of free cysteine or even to (re)generate active enzyme via protein turnover/expression during critical phases rather than through recycling by efficient enzymatic activities.

Experimental procedures

Protein expression, purification and sample preparation

The MTH711 ORF was generated from genomic DNA of *Methanothermobacter thermautotrophicus* strain *Delta H* (Archaeenzentrum, Univ. Regensburg, Germany) by PCR amplification and cloned into pET15b (Novagen). An MTH711 Cys69Ser and Cys112Ser double mutant was generated using the Invitrogen GeneTailor™ site directed mutagenesis system. MTH711 production was carried out in *E. coli* BL21(DE3)*pLysS* (Stratagene); expression was induced at an A_{600} of 0.7 by addition of 0.3 mM IPTG for 22 h at 20°C. For [^{15}N]- and [^{15}N,^{13}C]-labeled samples, cells were grown at 37 °C in M9 minimal media supplemented with $^{15}NH_4Cl$ as the sole nitrogen source and $^{13}C_6$-glucose, as the unique carbon source, respectively. Purification was carried out as described elsewhere (Carella et al., 2010).

The ILO and NHO ORFs where generated from the same source material as MTH711, inserted into pET15b, expressed in *E. coli* BL21(DE3) in LB media at an IPTG concentration of 1mM at 37 °C for three hours. Purification was carried out as described in (Amegbey et al., 2003, Bhattacharyya et al., 2002).

MSR enzyme activity assay

MSR activity was assayed as described previously (Hansel *et al.*, 2003, Jung *et al.*, 2002, Wassef et al., 2007) using a synthetic peptide with the sequence KIFM(O)K (MW 723; Jena Bioscience, Germany) and Met-(R)-SO or Met-(S)-SO, respectively. Oxidised peptide, Met-(R)-SO and Met-(S)-SO were derivatised with 2,4-dinitrofluorobenzene-ethanol (DNFB), which allowed their detection at 365 nm. The reaction mixture contained 100 µM peptide in 50 mM Tris/HCl (pH 7.4), 1 µM MTH711 and as electron donor either 10 mM

dithiothreitol (DTT) or 5 mM cysteine or 15 µg of human or *E. coli* thioredoxin (Sigma, Deisenhofen, Germany) or 200 µM of either ILO or NHO, respectively. Coenzyme M (Sigma, Deisenhofen, Germany) was used at 3 and 30 mM and under protective argon atmosphere. As controls, the peptide was incubated with either DTT or MTH711 only and the assay was performed also using the human MSRA (Jena Bioscience, Germany). The reactions were incubated for 1 hour at 45 °C with MTH711 and at 37 °C with 1 µM human MSRA. For the stereo-specificity assay, MTH711 was incubated either with Met-(R)-SO or Met-(S)-SO in the presence of 10 mM DTT. Samples were analysed using an ÄKTA system and a Source 15RPC-ST4.6/100 reverse phase column (GE Healthcare, Germany) developed in 20 min. with a flow rate of 1 mL/min employing a gradient starting with H_2O/0.1% trifluoroacetic acid to 84% acetonitrile/ 0.1% trifluoroacetic acid in H_2O. Absorption was monitored at 365 nm and a single peak corresponding to the oxidised (elution volume of 11.6 mL) or reduced peptide (elution volume 12.2 mL) or two peaks corresponding to the partially oxidised and partially reduced peptide were observed. For the assays depicted in Fig. 2J, K, L HPLC analysis using a 4.6x250mm Vydac 218TPC18 5µ column with a flow rate of 2mL/min and the same gradient as above was performed. Retention times as monitored at 365 nm were 12.6 min (corresponding to an elution vol. of 25.2 mL) for the oxidised and 12.9 min (corresponding to an elution vol. of 25.8 mL) for the reduced peptide.

Determination of cysteine sulfenic acid and thiol content

Cysteine sulfenic acid (Cys-SOH) content was determined using the specific 5–thio–2–nitrobenzoic acid (TNB) reagent prepared by reduction of 5,5'–dithio–bis(2–nitrobenzoic acid) (DTNB) (Turell *et al.*, 2008). MTH711 and its mutants were reduced by incubation with 10 mM DTT. Excess DTT was removed by buffer exchange using a NAP–5 column (GE Healthcare). Prereduced MTH711 (wild type and mutants; 7.5 µM and 12.5 µM) were

incubated with 70 µM TNB in a final volume of 100 µl 50 mM Tris-HCl, pH 8.0. Cys-SOH formation was monitored spectrophotometrically by observing the change in TNB^- concentration at 412 nm after addition of MetSO (10 mM) using a molar extinction coefficient of 14,150 $M^{-1}cm^{-1}$ (Tarrago et al., 2010). Reversal of the reaction was initiated by adding 20 mM DTT. Change in TNB^- concentration was again monitored at 412 nm. Quantification of Cys thiols was performed by using both 7.5 µM and 12.5 µM enzyme in the presence of 300 µM DTNB as described by (Boschi-Muller et al., 2000). Formation of TNB^- was followed at 412 nm and the thiol content was calculated using a molar extinction coefficient of 13,600 $M^{-1}cm^{-1}$. Absorbance was recorded using a Specord 210 UV/VIS spectrophotometer (Analytik Jena).

Mass spectrometry

The MALDI-TOF mass spectra were acquired using an UltraflexII Tof/Tof instrument (Bruker, Bremen, Germany). Sinapinic acid was used as the matrix in combination with an AnchorChip 800/384 target (Bruker, Bremen, Germany). Sample preparation was performed by the standard procedure as described in the AnchorChip manual. Protein amounts were in the range of 0.5 pmol to 5 pmol per anchor spot.

Extended X-ray absorption fine structure (EXAFS) analysis

XAS data were collected on 25 µL of a 1 mM MTH711 frozen solution up to 1000 eV above the Zn K-edge in fluorescence mode at the EMBL bending magnet beamline D2 (DESY, Hamburg, Germany) equipped with a Si(111) double crystal monochromator, a focusing mirror, and a 13 element Ge solid-state fluorescence detector (Canberra). The protein solution was filled into plastic sample holders covered with polyimid windows, frozen in liquid nitrogen, and kept at 20 K during the experiment. Harmonic rejection was achieved by a focusing mirror with a cut-off energy of 21 keV and a monochromator detuning to 70%

of peak intensity. While processing a pulse, the fluorescence detector was frozen (dead time). We ensured that no more than 20% of the counts occurred in this period and corrected each data point for this effect. The energy axis of each scan was calibrated using the Bragg reflections of a static Si(220) crystal in back-reflection geometry. Data analysis and reduction was performed with KEMP (Korbas *et al.*, 2006, Wellenreuther & Meyer-Klaucke, 2007) and initial automated data analysis with ABRA (Wellenreuther & Meyer-Klaucke, 2007). Based on the best model identified by ABRA's meta analysis (4 sulfur ligands) the EXAFS data were refined with EXCURVE (Binsted *et al.*, 1992). The best fit to the data comprised 4 sulfur ligands at 2.331 (2) Å with a Debye-Waller parameter ($2\sigma^2$) of 0.0069 (3) $Å^2$ and EF=-8.5 (4) eV using $E_{0,Zn}$=9662 eV. In parenthesis, the double standard deviation is given as an estimate for the error margins.

NMR spectroscopy

NMR spectra were acquired on Varian ^{UNITY}*INOVA* 600 MHz and 750 MHz spectrometers at 318 K. Data were processed with VNMR (Varian Inc., Palo Alto, USA) and analysed with XEASY (Bartels *et al.*, 1995) and CARA (Keller, 2004).

Following the protocol described in (Ohlenschlager *et al.*, 2006), resonance assignment was achieved by standard triple resonance experiments as detailed in (Carella et al., 2010). Combined ^{1}H and ^{15}N chemical shift differences were calculated using $\Delta\delta(ppm)=|\Delta\delta^{15}N|/f+|\Delta\delta^{1}H|$, where the scaling factor f=6.2 was used to normalise the ^{1}H and ^{15}N chemical shifts (Williamson *et al.*, 1997). Amide proton exchange rates were monitored by a series of [^{1}H-^{15}N]-HSQC experiments of 1 hour duration, performed over 24 hours. The amide groups were classified into three categories according to the time scale of ^{1}H/^{2}H exchange (Kim *et al.*, 1993): fast (complete exchange after re-dissolving the sample in $^{2}H_2O$), intermediate (significant exchange within 1-2 h), slow (no exchange, even after weeks).

Interproton distance restraints were derived from 3D [^{1}H,^{1}H,^{13}C]-NOESY-HSQC (100 ms mixing time) and 3D [^{1}H,^{1}H,^{15}N]-NOESY-HSQC spectra (80 ms mixing time). For the assignment of the aromatic protons a [^{1}H,^{1}H,^{13}C]-NOESY-HSQC (100 ms mixing time) was recorded with the ^{13}C frequency carrier set to 125 ppm (corresponding to the aromatic carbons).

Structure calculation and coordinates

Upper limit distance constraints for the non-exchangeable hydrogens were classified according to their intensity in the NOESY spectra corresponding to distance limits of 2.7, 3.2, 3.9, 4.8 and 5.5 Å, respectively. Nuclear Overhauser enhancement intensities corresponding to fixed $H^{\beta 2}$-$H^{\beta 3}$ and aromatic ring distances were used for calibration. Additional upper and lower limit constraints of 2.30-2.40 Å for the Zn-S^{γ} distances as derived from EXAFS and a range of 3.80-3.85 Å for the 4 sulfur-sulfur distances were included to maintain a tetrahedral geometry at the zinc site.

The 2428 experimental distances derived from NOE cross peaks were used as upper limit constraints in DYANA (Herrmann *et al.*, 2002). By including 124 $J_{HNH\alpha}$ coupling constants, 388 torsion angle constraints were obtained from local conformational analysis with the FOUND module (Guntert, 1998). Hydrogen bonds formed consistently during initial calculations, were included as additional 154 upper and lower limit constraints for final structure calculations.

Energy minimisation of the 20 out of 100 structures with the lowest DYANA target function was performed with the empirical force field Amber94 (Cornell *et al.*, 1995) using the 'conjugate gradient'-Method (Powell, 1977) as implemented in the program OPAL

(Luginbühl *et al.*, 1996). The quality of the structures was assessed by PROCHECK (Laskowski *et al.*, 1996). Figures were produced using MOLMOL (Koradi *et al.*, 1996).

^{15}N relaxation measurements

^{15}N relaxation data (T_1, T_2 and [^{1}H]-^{15}N steady-state heteronuclear NOE (HetNOE)) were recorded on a 750 MHz Bruker Avance III spectrometer and 318 K using a 0.65 mM ^{15}N-labelled sample of MTH711. The relaxation delays were applied in an interleaved fashion and set to 0, 0.002, 0.0025, 0.05, 0.10, 0.15, 0.20, 0.30, 0.50, 0.80, 1.00, 1.50 and 2.0 s for T_1 measurements and to 16.7, 33.4, 50.1, 66.8, 100.2, 133.6, 183.7, 233.8 ms for T_2 measurements. The recycle delay between transients was set to 3 s for T_1 and T_2 and to 5 s for the HetNOE. The heteronuclear NOE experiments were run in an interleaved fashion with and without (reference experiment) proton saturation during the recovery delay. The relaxation spectra were processed using TOPSPIN (Bruker Biospin) and NMRpipe (Delaglio *et al.*, 1995) and analysed using NMRDRAW (Delaglio et al., 1995). Relaxation curve fitting and data analysis was performed using the programs RELAXFIT, DYNAMICS (Fushman *et al.*, 1997, Hall & Fushman, 2003). [^{1}H]-^{15}N NOEs were determined as the peak intensity ratio between the reference and the saturation experiment. The uncertainty in the HetNOE values was set to 5% of their values (Viles *et al.*, 2001).

Data Bank accession codes

Coordinates and chemical shift data have been deposited in the Brookhaven Protein Data Bank (accession code 2K8D) and the BioMagResBank (accession number 15941).

Acknowledgements

We are grateful to H. Huber (Archaeenzentrum Regensburg) for providing *M. thermoautotrophicus* cells, A. Hansel (FSU Jena) for the peptide and MetSO enantiomers, M. Baum (FLI) for technical assistance, and J. Wöhnert (Univ. Frankfurt) for critical reading of the manuscript. This work was supported in part by the DFG Research Training Group "768 Biomolecular Switches". The Fritz Lipmann Institute is financially supported by the State of Thuringia and the Federal Government of Germany.

Figure Legends

Figure 1. Alignment of representative sequences of MSRB enzymes. The sequences of *M. thermoautotrophicus* (MTH711; GeneID 1470672), human MSRB 2 and 3 (hMSRB2 and hMSRB3; GeneID 22921 and 253827), *E. coli* (Ecoli, GeneID 947188), *S. elongatus* (Synel, GeneID 6056502), *Drosophila melanogaster* (Drome, GeneID 41309), *Xanthomonas campestris* (Xanca, GeneID 6223654) *Burkholderia pseudomallei* (Burps, GeneID 3690705), PilB of *N. gonorrhoeae* (Neigo, GeneID 3282737) and *B. subtilis* (Bacsu, GeneID 939102) were aligned with ClustalW (URL: http://www.ebi.ac.uk/Tools/clustalw2/index.html). The numbering of amino acid residues indicated is based on the numbering of the *M. thermautotrophicus* MTH711 sequence. (Magenta) conserved catalytic cysteine; (blue) Zn^{2+}-binding site and (grey) corresponding residues in the zinc-free enzymes; (green) semiconserved "recycling" cysteine; (yellow) conserved residues in the active site; (orange) two additional Cys in MTH711 discussed in the text. The secondary structure elements found in MTH711 are indicated as blue arrows (β strand) and red cylinders (α helix).

Figure 2. MTH711 MetSO reductase activity. MTH711 activity was assayed by using Met-(R)-SO, Met-(S)-SO or a KIFM(O)K peptide as substrate. Reaction products were separated on a reverse phase column (for details see Experimental Procedures). Note that for either substrate, the elution of the oxidised species preceeds the one for the reduced species. Elution profiles are shown. (A) MTH711 reduces Met-(R)-SO to Met (blue) but not Met-(S)-SO (red). (B) The oxidised peptide elutes at 11.6 mL. (C) DTT does not reduce the oxidised peptide. (D) MTH711 as well as (E) MSRA and (F) MTH711 or MSRA do not reduce the oxidised peptide in absence of DTT. (G) MTH711 in the presence of DTT partially reduces the oxidised peptide and leads to a second peak at 12.2 mL, corresponding to the reduced peptide. (H) MSRA in the presence of DTT partially reduces the oxidised peptide as well and leads to

a second peak at 12.2 mL corresponding to the reduced peptide. (I) The peptide is completely reduced in the presence of MTH711, MSRA and DTT giving rise to a single peak eluting at 12.2 mL. (J) MTH711 is active in the presence of free cysteine. The C68S and C112S double mutant of MTH711 (MTH2xmut) is active in the presence of (K) free cysteine and (L) DTT. Experiments depicted in panels J, K and M were carried out on a HPLC (see Experimental Procedures). Hence, the elution volumes differ from the ones shown in the other panels: oxidised peptide elutes at 25.2 mL prior to the reduced peptide at 25.8 mL. (M) MTH711 in the presence of either Trx-homologue NHO (red) or ILO (blue) does not reduce the oxidised peptide, while (N) MSRA reduces the oxidised peptide to some extend in the presence of NHO (red) but not of ILO (blue). (O) MTH711 in the presence of either human (red) or *E. coli* (blue) Trx does not reduce the oxidised peptide, while (P) MSRA reduces the oxidised peptide in the presence of either human (red) or *E. coli* (blue) Trx.

Figure 3. NMR spectroscopy of MTH711. (A) Superimposed 750 MHz [^{1}H,^{15}N]-HSQC spectra of 100 µM MTH711 in NMR buffer at pH 7.2 and 318 K (45 °C) reduced by 100 mM DTT (blue contours) or oxidised by 20 mM MetSO (red contours). The residues undergoing a combined chemical [^{1}H,^{15}N] shift perturbation of more than 0.1 ppm are indicated by residue labels and connected by a solid line. **(**B) The 750 MHz [^{1}H,^{15}N]-HSQC spectrum of 1.2 mM oxidised MTH711 in NMR buffer at pH 7.2 and 318 K (45 °C). Assignments for 133 of the clearly resolved peaks are indicated. The unlabelled peaks could not be unambiguously assigned due to fast exchange or spectral overlap. Side-chain amide resonances are connected by hatched lines. Inset: central region (boxed) of the spectrum expanded for clarity.

Figure 4. Quantification of cysteine sulfenic acid in MTH711. Prereduced MTH711 wild type (red), the C69S/C112S double mutant (blue) and the active site C139S mutant (green)

(each at 7.5 µM) were incubated with 70 µM TNB and TNB oxidation was monitored at 412 nm. After 3 min. 10 mM MetSO was added (black arrow) and the absorbance monitored in 20 sec. intervals until at least 3 min of constant absorbance was observed. Subsequently the reactions were supplemented with 20 mM DTT (red and blue arrows) and the absorption was followed until no further change occurred. The molar amount of oxidised TNB^- produced during the reaction was calculated from the difference in absorption between the starting value at 3 min. and the plateau value after adding MetSO using the molar extinction coefficient of 14,150 $M^{-1}cm^{-1}$.

Figure 5. EXAFS analysis of the MTH711 zinc coordinating centre. EXAFS and corresponding Fourier transform for MTH711. (A) The EXAFS signal is dominated by a single frequency, corresponding to one major peak in (B) the Fourier transform. In the refinement this is identified as back-scattering from 4 sulfur ions, representing the 4 zinc coordinating S^{γ} of the indicated Cys residues shown schematically in (B).

Figure 6. Solution structure of oxidised MTH711. (A) Overall solution structure of MTH711. Superimposition of the backbone traces by fitting the well-defined β-strand regions of the 20 energy minimised structures with the lowest DYANA target function. Residues at the N- and C-termini (M4 and G154) as well as other residues including the active site Cys (C139) and two of the four zinc co-ordinating Cys (C70 and C119) are indicated. (B) Stereo view generated in MOLMOL (Koradi et al., 1996) of a ribbon representation of the structure closest to the mean. The catalytic cysteine (magenta), the zinc ion (yellow sphere) and the zinc coordinating Cys side chains (orange) are highlighted. The distance (15 Å) between the active site and the Zn^{2+}-ion is indicated. (C) Close–up of the MTH711 active site. Amino acids that define the active site are the catalytic cysteine (magenta) and the conserved residues surrounding the catalytic cysteine (yellow). (D) The two cysteines present outside of the

active site and not involved in zinc binding are Cys69 (green) and Cys112 (yellow). The distance to the active site Cys139 (magenta) is also indicated.

Figure 7. Dynamics of MTH711. Order parameters S^2 of the MTH711 backbone as derived from T_1, T_2 relaxation times and the [^{1}H]-^{15}N-NOE data acquired at 750 MHz and 318K (45 °C). The secondary structure elements (β-sheets as blue arrows, α-helices as red cylinders) of MTH711 are indicated.

Figure 8. Comparison between zinc free and zinc containing MSRBs. Superimposition of the backbone traces of the PilB crystal structure (green trace, pdb 1L1D) of *N. gonorrhoeae* and of the MTH711 NMR solution structure (red trace, pdb 2K8D). Active site and the zinc ion binding site in MTH711 are indicated by arrows and the termini (N-terminus, C-terminus) are labelled.

Figure 9. Chemical shift perturbation of MTH711 backbone amides upon interconversion between the oxidised and the reduced state. (A) Combined ^{1}H and ^{15}N chemical shift differences were calculated according to (Williamson et al., 1997). The graph shows the calculated chemical shift differences over the entire sequence. Residues showing a combined chemical shift perturbation of $\Delta\delta > 0.1$ppm (hatched line) are Thr48, Glu49, Ser89, Arg102, Glu103, Asp104, Arg111, Cys112, His125, Phe127, Asp128, Met140, Asn141, Ser142 and Ala143. (B) Mapping of chemical shift perturbations of $\Delta\delta > 0.1$ppm (yellow) onto the main chain structure of MTH711. Active site Cys139 (magenta), Cys69 (green) and Cys112 (yellow) are indicated.

Table 1. MALDI–TOF mass spectrometry of reduced and oxidised MTH711

	Mass Calculated (Da)	Mass Observed (Da)	Mass Difference *(obs–calc;* Da*)*	Mass Difference (*ox–red;* Da)
Major peak[1)]				
Reduced (100 mM DTT)	16,686	16,692	6	16
Oxidised (20 mM MetSO)	16,702	16,708	6	
Minor peak[2)]				
Reduced (100 mM DTT)	16,751	16,755	4	14
Oxidised (20 mM MetSO)	16,767	16,769	2	

1) Calculated mass corresponds to MTH711 without zinc

2) Calculated mass corresponds to MTH711 containing zinc (mass: 65 Da)

Table 2. EXAFS, NMR and refinement statistics for the MTH711 structure

EXAFS refinement statistics[1)]		2σ e.m.[2)]
Ligands	4 S	
R (Å)	2.33	0.002
2 σ^2 (Å^2)	0.0069	0.00003
EF	-8.5	0.04
R_{EXAFS}	25.77	

NMR distance & dihedral constraints	
Distance constraints	2428
Hydrogen bond constraints	154
Zinc geometry constraints	18
Total dihedral angle constraints	388

Structure statistics		
Violations	Mean	s.d.[3)]
Target function (Å^2)	5.34	0.32
Distance constraints (Å)	10.74	0.84
Max. distance constraints violation (Å)	0.32	0.05
Dihedral angle constraints (°)	42.44	10.10
Max. dihedral angle violations (°)	6.00	1.46
AMBER physical energies (kcal mol^{-1})	-2245.26	97.44
Deviations from idealized geometry		
Bond lengths (Å)	0.0057	0.0064
Bond angles (°)	1.6232	0.0001
Mean global r.m.s.d. (Å)		
Heavy atom (residues 6-49,61-154)	1.33	0.28
Backbone atoms (residues 6-49,61-154)	0.80	0.24

1) Only the best model is presented. R: inter-atomic distance, 2 σ^2: Debye-Waller factor, EF: Fermi Energy, the shift of the origin energy with respect to E_0=9662 eV.

2) e.m.: error margin

3) s.d.: standard deviation

References

Amegbey, G. Y., H. Monzavi, B. Habibi-Nazhad, S. Bhattacharyya & D. S. Wishart, (2003) Structural and functional characterization of a thioredoxin-like protein (Mt0807) from Methanobacterium thermoautotrophicum. *Biochemistry* **42**: 8001-8010.

Auld, D. S., (2001) Zinc coordination sphere in biochemical zinc sites. *Biometals* **14**: 271-313.

Balch, W. E. & R. S. Wolfe, (1979) Specificity and biological distribution of coenzyme M (2-mercaptoethanesulfonic acid). *J Bacteriol* **137**: 256-263.

Bartels, C., T. H. Billeter, P. Güntert & K. Wüthrich, (1995) The program XEASY for computer-supported NMR spectral analysis of biological macromolecules. *J Biomolecular NMR* **5**: 1-10.

Bartlett, R. K., R. J. Bieber Urbauer, A. Anbanandam, H. S. Smallwood, J. L. Urbauer & T. C. Squier, (2003) Oxidation of Met144 and Met145 in calmodulin blocks calmodulin dependent activation of the plasma membrane Ca-ATPase. *Biochemistry* **42**: 3231-3238.

Beckman, K. B. & B. N. Ames, (1998) The free radical theory of aging matures. *Physiol Rev* **78**: 547-581.

Berlett, B. S. & E. R. Stadtman, (1997) Protein oxidation in aging, disease, and oxidative stress. *J Biol Chem* **272**: 20313-20316.

Bhattacharyya, S., B. Habibi-Nazhad, G. Amegbey, C. M. Slupsky, A. Yee, C. Arrowsmith & D. S. Wishart, (2002) Identification of a novel archaebacterial thioredoxin: determination of function through structure. *Biochemistry* **41**: 4760-4770.

Bigelow, D. J. & T. C. Squier, (2005) Redox modulation of cellular signaling and metabolism through reversible oxidation of methionine sensors in calcium regulatory proteins. *Biochim Biophys Acta* **1703**: 121-134.

Binsted, N., R. W. Strange & S. S. Hasnain, (1992) Constrained and restrained refinement in EXAFS data analysis with curved wave theory. *Biochemistry* **31**: 12117-12125.

Boschi-Muller, S., S. Azza, S. Sanglier-Cianferani, F. Talfournier, A. Van Dorsselear & G. Branlant, (2000) A sulfenic acid enzyme intermediate is involved in the catalytic mechanism of peptide methionine sulfoxide reductase from Escherichia coli. *J Biol Chem* **275**: 35908-35913.

Boschi-Muller, S., A. Gand & G. Branlant, (2008) The methionine sulfoxide reductases: Catalysis and substrate specificities. *Arch Biochem Biophys* **474**: 266-273.

Boschi-Muller, S., A. Olry, M. Antoine & G. Branlant, (2005) The enzymology and biochemistry of methionine sulfoxide reductases. *Biochim Biophys Acta* **1703**: 231-238.

Carella, M., O. Ohlenschlager, R. Ramachandran & M. Gorlach, (2010) 1H, 13C and 15N resonance assignment of a zinc-binding methionine sulfoxide reductase type-B from the thermophilic archeabacterium Methanothermobacter thermoautotrophicus. *Biomol NMR Assign* **4**: 93-95.

Claiborne, A., H. Miller, D. Parsonage & R. P. Ross, (1993) Protein-sulfenic acid stabilization and function in enzyme catalysis and gene regulation. *FASEB J* **7**: 1483-1490.

Cornell, W. D., P. Cieplak, C. I. Bayly, I. R. Gould, K. M. Merz, D. M. Ferguson, D. C. Spellmeyer, T. Fox, J. W. Caldwell & P. A. Kollman, (1995) A second generation force field for the simulation of proteins, nucleic acids and organic molecules. *J Am Chem Soc* **117**: 5179-5197.

Coudevylle, N., M. Antoine, S. Bouguet-Bonnet, P. Mutzenhardt, S. Boschi-Muller, G. Branlant & M. T. Cung, (2007) Solution structure and backbone dynamics of the reduced form and an oxidized form of E. coli methionine sulfoxide reductase A (MsrA): structural insight of the MsrA catalytic cycle. *J Mol Biol* **366**: 193-206.

D'Autreaux, B. & M. B. Toledano, (2007) ROS as signalling molecules: mechanisms that generate specificity in ROS homeostasis. *Nat Rev Mol Cell Biol* **8**: 813-824.

Delaglio, F., S. Grzesiek, G. W. Vuister, G. Zhu, J. Pfeifer & A. Bax, (1995) NMRPipe: a multidimensional spectral processing system based on UNIX pipes. *Journal of biomolecular NMR* **6**: 277-293.

Delaye, L., A. Becerra, L. Orgel & A. Lazcano, (2007) Molecular evolution of peptide methionine sulfoxide reductases (MsrA and MsrB): on the early development of a mechanism that protects against oxidative damage. *J Mol Evol* **64**: 15-32.

Erickson, J. R., M. L. Joiner, X. Guan, W. Kutschke, J. Yang, C. V. Oddis, R. K. Bartlett, J. S. Lowe, S. E. O'Donnell, N. Aykin-Burns, M. C. Zimmerman, K. Zimmerman, A. J. Ham, R. M. Weiss, D. R. Spitz, M. A. Shea, R. J. Colbran, P. J. Mohler & M. E. Anderson, (2008) A dynamic pathway for calcium-independent activation of CaMKII by methionine oxidation. *Cell* **133**: 462-474.

Fahey, R. C., (2001) Novel thiols of prokaryotes. *Annu Rev Microbiol* **55**: 333-356.

Finkel, T., (2003) Oxidant signals and oxidative stress. *Curr Opin Cell Biol* **15**: 247-254.

Fukushima, E., Y. Shinka, T. Fukui, H. Atomi & T. Imanaka, (2007) Methionine sulfoxide reductase from the hyperthermophilic archaeon Thermococcus kodakaraensis, an enzyme designed to function at suboptimal growth temperatures. *J Bacteriol* **189**: 7134-7144.

Fushman, D., S. Cahill & D. Cowburn, (1997) The main-chain dynamics of the dynamin pleckstrin homology (PH) domain in solution: analysis of 15N relaxation with monomer/dimer equilibration. *J Mol Biol* **266**: 173-194.

Giorgio, M., M. Trinei, E. Migliaccio & P. G. Pelicci, (2007) Hydrogen peroxide: a metabolic by-product or a common mediator of ageing signals? *Nat Rev Mol Cell Biol* **8**: 722-728.

Glaser, C. B., J. Morser, J. H. Clarke, E. Blasko, K. McLean, I. Kuhn, R. J. Chang, J. H. Lin, L. Vilander, W. H. Andrews & et al., (1992) Oxidation of a specific methionine in thrombomodulin by activated neutrophil products blocks cofactor activity. A potential rapid mechanism for modulation of coagulation. *J Clin Invest* **90**: 2565-2573.

Glaser, C. B., G. Yamin, V. N. Uversky & A. L. Fink, (2005) Methionine oxidation, alpha-synuclein and Parkinson's disease. *Biochim Biophys Acta* **1703**: 157-169.

Guntert, P., (1998) Structure calculation of biological macromolecules from NMR data. *Q Rev Biophys* **31**: 145-237.

Hall, J. B. & D. Fushman, (2003) Characterization of the overall and local dynamics of a protein with intermediate rotational anisotropy: Differentiating between conformational exchange and anisotropic diffusion in the B3 domain of protein G. *Journal of biomolecular NMR* **27**: 261-275.

Halliwell, B. & J. M. C. Gutteridge, (1999) Free Radicals in Biology and Medicine. *Oxford Universty Press* **4th ed.**

Hansel, A., S. H. Heinemann & T. Hoshi, (2005) Heterogeneity and function of mammalian MSRs: enzymes for repair, protection and regulation. *Biochim Biophys Acta* **1703**: 239-247.

Hansel, A., S. Jung, T. Hoshi & S. H. Heinemann, (2003) A second human methionine sulfoxide reductase (hMSRB2) reducing methionine-R-sulfoxide displays a tissue expression pattern distinct from hMSRB1. *Redox Rep* **8**: 384-388.

Herrmann, T., P. Guntert & K. Wuthrich, (2002) Protein NMR structure determination with automated NOE assignment using the new software CANDID and the torsion angle dynamics algorithm DYANA. *J Mol Biol* **319**: 209-227.

Hoshi, T. & S. Heinemann, (2001) Regulation of cell function by methionine oxidation and reduction. *J Physiol* **531**: 1-11.

Jacob, C., G. I. Giles, N. M. Giles & H. Sies, (2003) Sulfur and selenium: the role of oxidation state in protein structure and function. *Angew Chem Int Ed Engl* **42**: 4742-4758.

Johnson, D. & J. Travis, (1979) The oxidative inactivation of human alpha-1-proteinase inhibitor. Further evidence for methionine at the reactive center. *J Biol Chem* **254**: 4022-4026.

Jung, S., A. Hansel, H. Kasperczyk, T. Hoshi & S. H. Heinemann, (2002) Activity, tissue distribution and site-directed mutagenesis of a human peptide methionine sulfoxide reductase of type B: hCBS1. *FEBS Lett* **527**: 91-94.

Keller, R., (2004) The computer aided resonance assignment tutorial. *Cantina Verlag*.

Kettenhofen, N. J. & M. J. Wood, (2010) Formation, Reactivity, and Detection of Protein Sulfenic Acids. *Chem Res Toxicol*.

Kim, H. Y. & V. N. Gladyshev, (2004) Methionine sulfoxide reduction in mammals: characterization of methionine-R-sulfoxide reductases. *Mol Biol Cell* **15**: 1055-1064.

Kim, K. S., J. A. Fuchs & C. K. Woodward, (1993) Hydrogen exchange identifies native-state motional domains important in protein folding. *Biochemistry* **32**: 9600-9608.

Koradi, R., M. Billeter & K. Wuthrich, (1996) MOLMOL: a program for display and analysis of macromolecular structures. *J Mol Graph* **14**: 51-55, 29-32.

Korbas, M., D. Fulla Marsa & W. Meyer-Klaucke, (2006) KEMP: A program script for automated biological x-ray absorption spectroscopy data reduction. *Rev. Sci. Instrum.* **77**: 063105 (063105 pages).

Kornhaber, G. J., D. Snyder, H. N. Moseley & G. T. Montelione, (2006) Identification of zinc-ligated cysteine residues based on 13Calpha and 13Cbeta chemical shift data. *Journal of biomolecular NMR* **34**: 259-269.

Kumar, R. A., A. Koc, R. L. Cerny & V. N. Gladyshev, (2002) Reaction mechanism, evolutionary analysis, and role of zinc in Drosophila methionine-R-sulfoxide reductase. *J Biol Chem* **277**: 37527-37535.

Laskowski, R. A., J. A. Rullmannn, M. W. MacArthur, R. Kaptein & J. M. Thornton, (1996) AQUA and PROCHECK-NMR: programs for checking the quality of protein structures solved by NMR. *Journal of biomolecular NMR* **8**: 477-486.

Levine, R. L., L. Mosoni, B. S. Berlett & E. R. Stadtman, (1996) Methionine residues as endogenous antioxidants in proteins. *Proc Natl Acad Sci U S A* **93**: 15036-15040.

Lipari, G. & A. Szabo, (1981) Nuclear magnetic resonance relaxation in nucleic acid fragments: models for internal motion. *Biochemistry* **20**: 6250-6256.

Lowther, W. T., H. Weissbach, F. Etienne, N. Brot & B. W. Matthews, (2002) The mirrored methionine sulfoxide reductases of Neisseria gonorrhoeae pilB. *Nat Struct Biol* **9**: 348-352.

Luginbühl, P., P. Güntert, M. Billeter & W. K, (1996) The new program OPAL for molecular dynamics simulations and energy refinements of biological macromolecules. *Journal of biomolecular NMR* **8**: 136-146.

Moskovitz, J., (2005) Methionine sulfoxide reductases: ubiquitous enzymes involved in antioxidant defense, protein regulation, and prevention of aging-associated diseases. *Biochim Biophys Acta* **1703**: 213-219.

Neiers, F., A. Kriznik, S. Boschi-Muller & G. Branlant, (2004) Evidence for a new sub-class of methionine sulfoxide reductases B with an alternative thioredoxin recognition signature. *J Biol Chem* **279**: 42462-42468.

Ohlenschlager, O., T. Seiboth, H. Zengerling, L. Briese, A. Marchanka, R. Ramachandran, M. Baum, M. Korbas, W. Meyer-Klaucke, M. Durst & M. Gorlach, (2006) Solution structure of the partially folded high-risk human papilloma virus 45 oncoprotein E7. *Oncogene* **25**: 5953-5959.

Olry, A., S. Boschi-Muller, M. Marraud, S. Sanglier-Cianferani, A. Van Dorsselear & G. Branlant, (2002) Characterization of the methionine sulfoxide reductase activities of PILB, a probable virulence factor from Neisseria meningitidis. *J Biol Chem* **277**: 12016-12022.

Olry, A., S. Boschi-Muller, H. Yu, D. Burnel & G. Branlant, (2005) Insights into the role of the metal binding site in methionine-R-sulfoxide reductases B. *Protein Sci* **14**: 2828-2837.

Petropoulos, I. & B. Friguet, (2006) Maintenance of proteins and aging: the role of oxidized protein repair. *Free Radic Res* **40**: 1269-1276.

Poole, L. B., P. A. Karplus & A. Claiborne, (2004) Protein sulfenic acids in redox signaling. *Annu Rev Pharmacol Toxicol* **44**: 325-347.

Powell, M., (1977) Restart procedures for the conjugate gradient method. *Math. prog.* **12**: 241-254.

Ranaivoson, F. M., M. Antoine, B. Kauffmann, S. Boschi-Muller, A. Aubry, G. Branlant & F. Favier, (2008) A structural analysis of the catalytic mechanism of methionine sulfoxide reductase A from Neisseria meningitidis. *J Mol Biol* **377**: 268-280.

Ranaivoson, F. M., F. Neiers, B. Kauffmann, S. Boschi-Muller, G. Branlant & F. Favier, (2009) Methionine sulfoxide reductase B displays a high level of flexibility. *J Mol Biol* **394**: 83-93.

Sagher, D., D. Brunell, J. F. Hejtmancik, M. Kantorow, N. Brot & H. Weissbach, (2006) Thionein can serve as a reducing agent for the methionine sulfoxide reductases. *Proc Natl Acad Sci U S A* **103**: 8656-8661.

Schoneich, C., (2005) Methionine oxidation by reactive oxygen species: reaction mechanisms and relevance to Alzheimer's disease. *Biochim Biophys Acta* **1703**: 111-119.

Shchedrina, V. A., G. Vorbruggen, B. C. Lee, H. Y. Kim, H. Kabil, L. G. Harshman & V. N. Gladyshev, (2009) Overexpression of methionine-R-sulfoxide reductases has no influence on fruit fly aging. *Mech Ageing Dev* **130**: 429-443.

Smith, D. R., L. A. Doucette-Stamm, C. Deloughery, H. Lee, J. Dubois, T. Aldredge, R. Bashirzadeh, D. Blakely, R. Cook, K. Gilbert, D. Harrison, L. Hoang, P. Keagle, W. Lumm, B. Pothier, D. Qiu, R. Spadafora, R. Vicaire, Y. Wang, J. Wierzbowski, R. Gibson, N. Jiwani, A. Caruso, D. Bush, J. N. Reeve & et al., (1997) Complete genome sequence of Methanobacterium thermoautotrophicum deltaH: functional analysis and comparative genomics. *J Bacteriol* **179**: 7135-7155.

Sohal, R. S., (2002) Oxidative stress hypothesis of aging. *Free Radic Biol Med* **33**: 573-574.

Stadtman, E. R. & B. S. Berlett, (1997) Reactive oxygen-mediated protein oxidation in aging and disease. *Chem Res Toxicol* **10**: 485-494.

Stadtman, E. R., J. Moskovitz & R. L. Levine, (2003) Oxidation of methionine residues of proteins: biological consequences. *Antioxid Redox Signal* **5**: 577-582.

Stadtman, E. R., H. Van Remmen, A. Richardson, N. B. Wehr & R. L. Levine, (2005) Methionine oxidation and aging. *Biochim Biophys Acta* **1703**: 135-140.

Tarrago, L., E. Laugier, M. Zaffagnini, C. Marchand, P. Le Marechal, N. Rouhier, S. D. Lemaire & P. Rey, (2009) Regeneration mechanisms of Arabidopsis thaliana methionine sulfoxide reductases B by glutaredoxins and thioredoxins. *J Biol Chem* **284**: 18963-18971.

Tarrago, L., E. Laugier, M. Zaffagnini, C. H. Marchand, P. Le Marechal, S. D. Lemaire & P. Rey, (2010) Plant thioredoxin CDSP32 regenerates 1-cys methionine sulfoxide reductase B activity through the direct reduction of sulfenic acid. *J Biol Chem* **285**: 14964-14972.

Thauer, R. K., A. K. Kaster, H. Seedorf, W. Buckel & R. Hedderich, (2008) Methanogenic archaea: ecologically relevant differences in energy conservation. *Nat Rev Microbiol* **6**: 579-591.

Turell, L., H. Botti, S. Carballal, G. Ferrer-Sueta, J. M. Souza, R. Duran, B. A. Freeman, R. Radi & B. Alvarez, (2008) Reactivity of sulfenic acid in human serum albumin. *Biochemistry* **47**: 358-367.

Viles, J. H., D. Donne, G. Kroon, S. B. Prusiner, F. E. Cohen, H. J. Dyson & P. E. Wright, (2001) Local structural plasticity of the prion protein. Analysis of NMR relaxation dynamics. *Biochemistry* **40**: 2743-2753.

Vogt, W., (1995) Oxidation of methionyl residues in proteins: tools, targets, and reversal. *Free Radic Biol Med* **18**: 93-105.

Wassef, R., R. Haenold, A. Hansel, N. Brot, S. H. Heinemann & T. Hoshi, (2007) Methionine sulfoxide reductase A and a dietary supplement S-methyl-L-cysteine prevent Parkinson's-like symptoms. *J Neurosci* **27**: 12808-12816.

Weissbach, H., F. Etienne, T. Hoshi, S. H. Heinemann, W. T. Lowther, B. Matthews, G. St John, C. Nathan & N. Brot, (2002) Peptide methionine sulfoxide reductase: structure, mechanism of action, and biological function. *Arch Biochem Biophys* **397**: 172-178.

Wellenreuther, G. & W. Meyer-Klaucke, (2007) Towards a Black-Box for Biological EXAFS Data Analysis - I. Identification of Zinc Finger Proteins. In: X-RAY ABSORPTION FINE STRUCTURE - XAFS13: 13th International Conference. pp. 322-324.

Williamson, R. A., M. D. Carr, T. A. Frenkiel, J. Feeney & R. B. Freedman, (1997) Mapping the binding site for matrix metalloproteinase on the N-terminal domain of the tissue inhibitor of metalloproteinases-2 by NMR chemical shift perturbation. *Biochemistry* **36**: 13882-13889.

Wong, Y. Q., K. J. Binger, G. J. Howlett & M. D. Griffin, (2010) Methionine oxidation induces amyloid fibril formation by full-length apolipoprotein A-I. *Proc Natl Acad Sci U S A* **107**: 1977-1982.

Figure 1

Carella, M et al. 2011
Molecular Microbiology
Accepted Manuscript Version

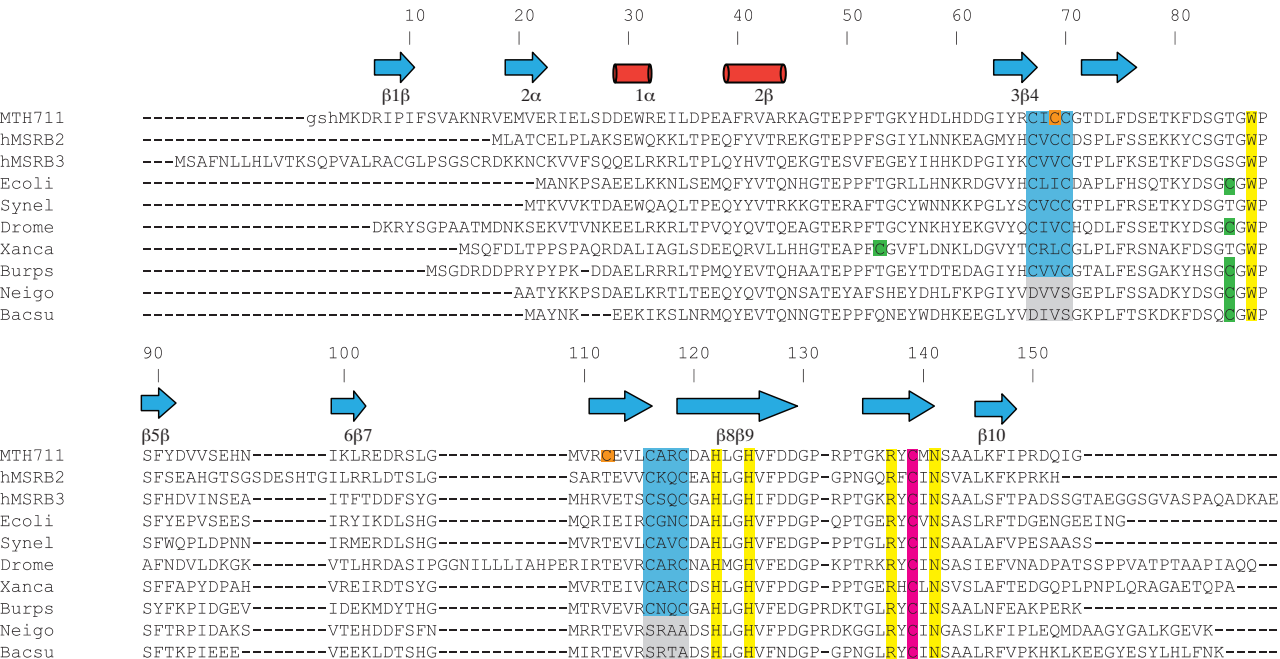

Figure 2

Carella, M et al. 2011
Molecular Microbiology
Accepted Manuscript Version

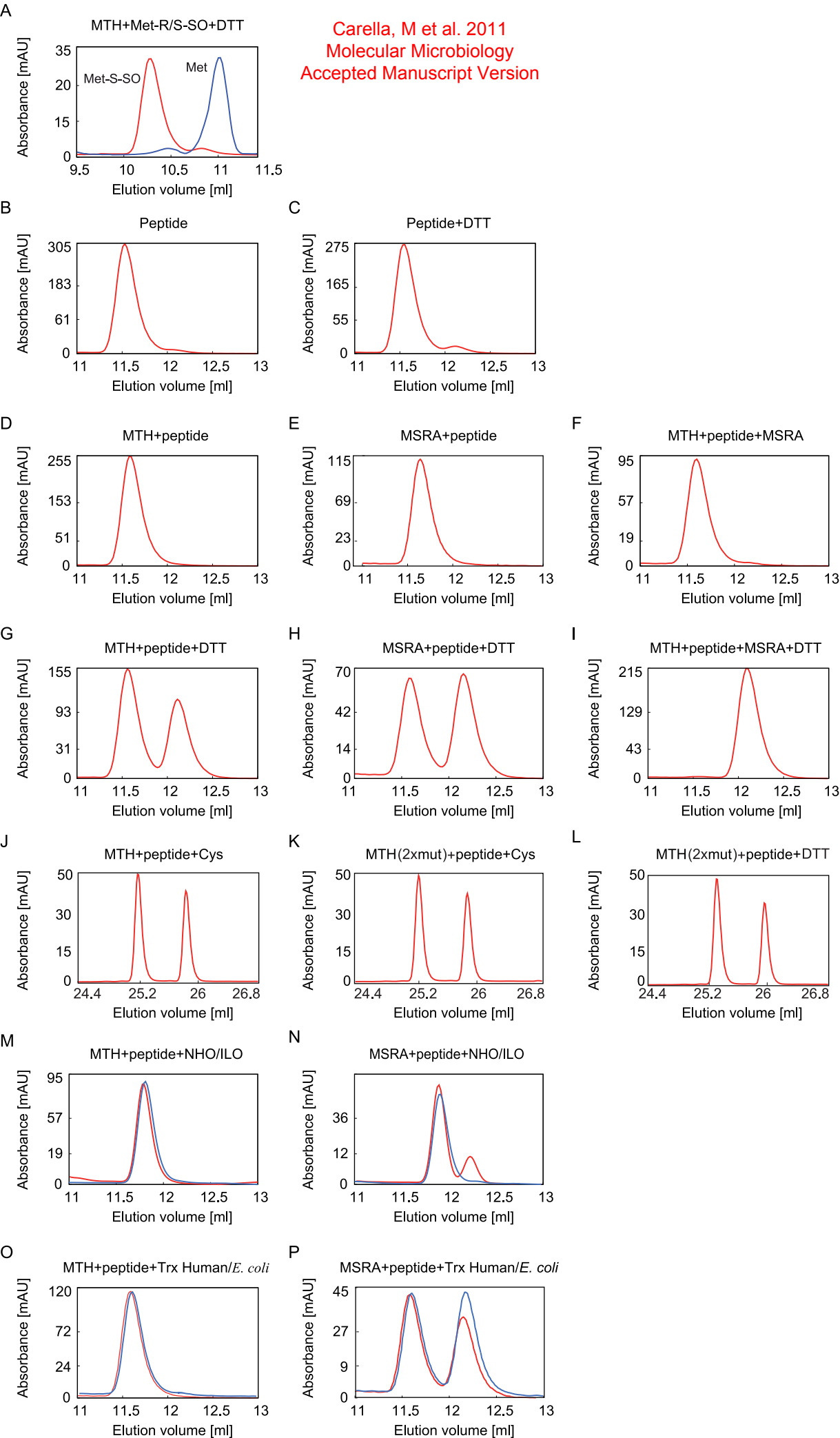

Figure 2

Carella, M et al. 2011
Molecular Microbiology
Accepted Manuscript Version

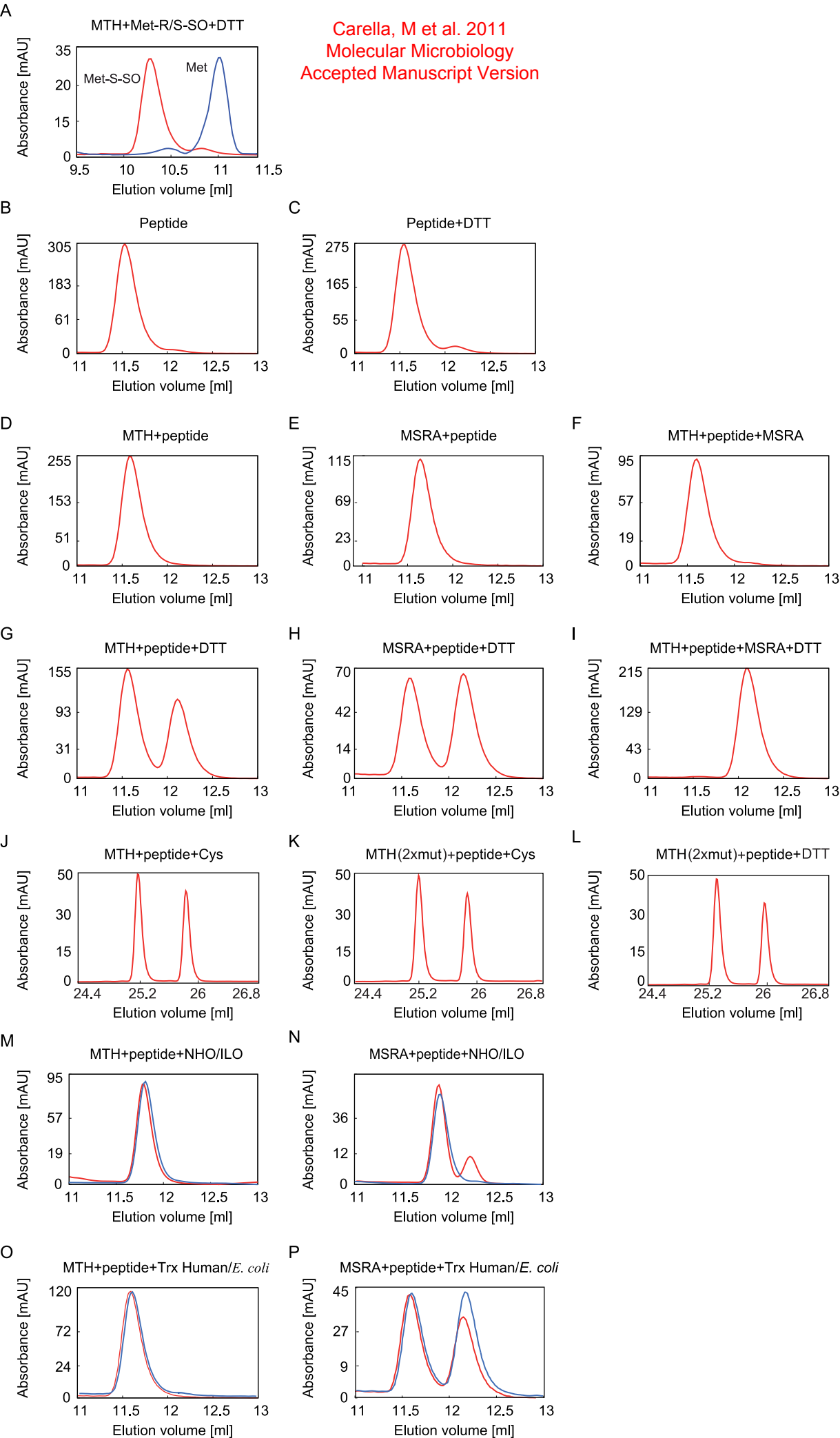

Figure 3

Carella, M et al. 2011
Molecular Microbiology
Accepted Manuscript Version

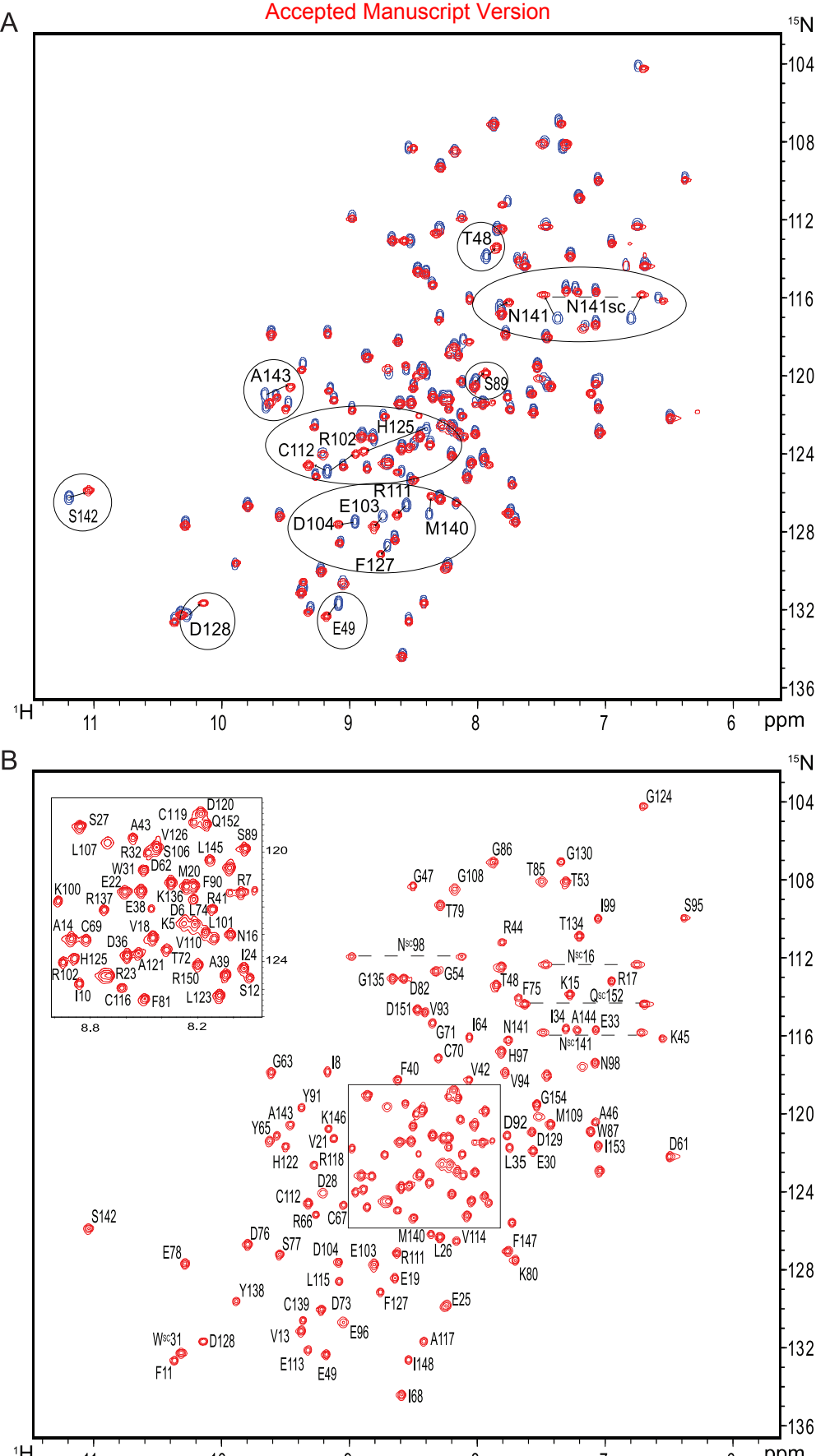

Figure 4

Carella, M et al. 2011
Molecular Microbiology
Accepted Manuscript Version

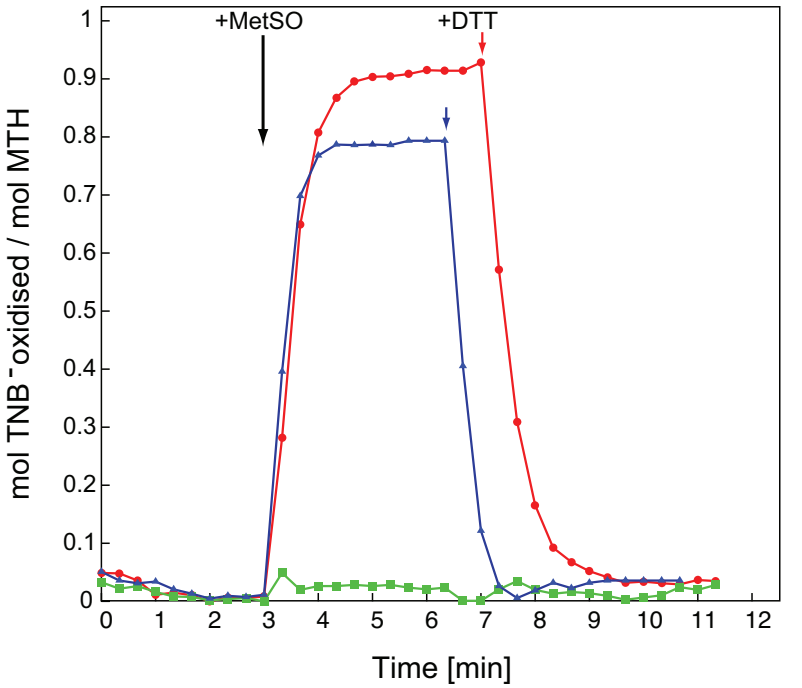

Figure 5

Carella, M et al. 2011
Molecular Microbiology
Accepted Manuscript Version

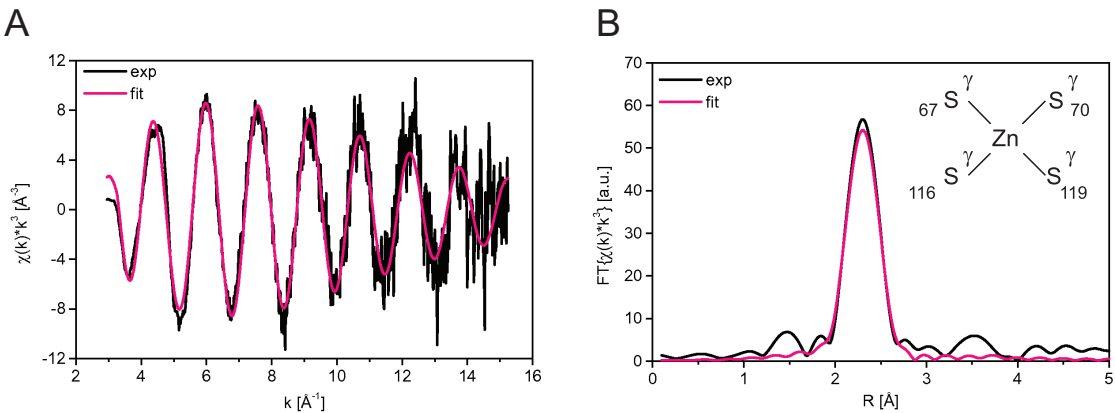

Figure 6

Carella, M et al. 2011
Molecular Microbiology
Accepted Manuscript Version

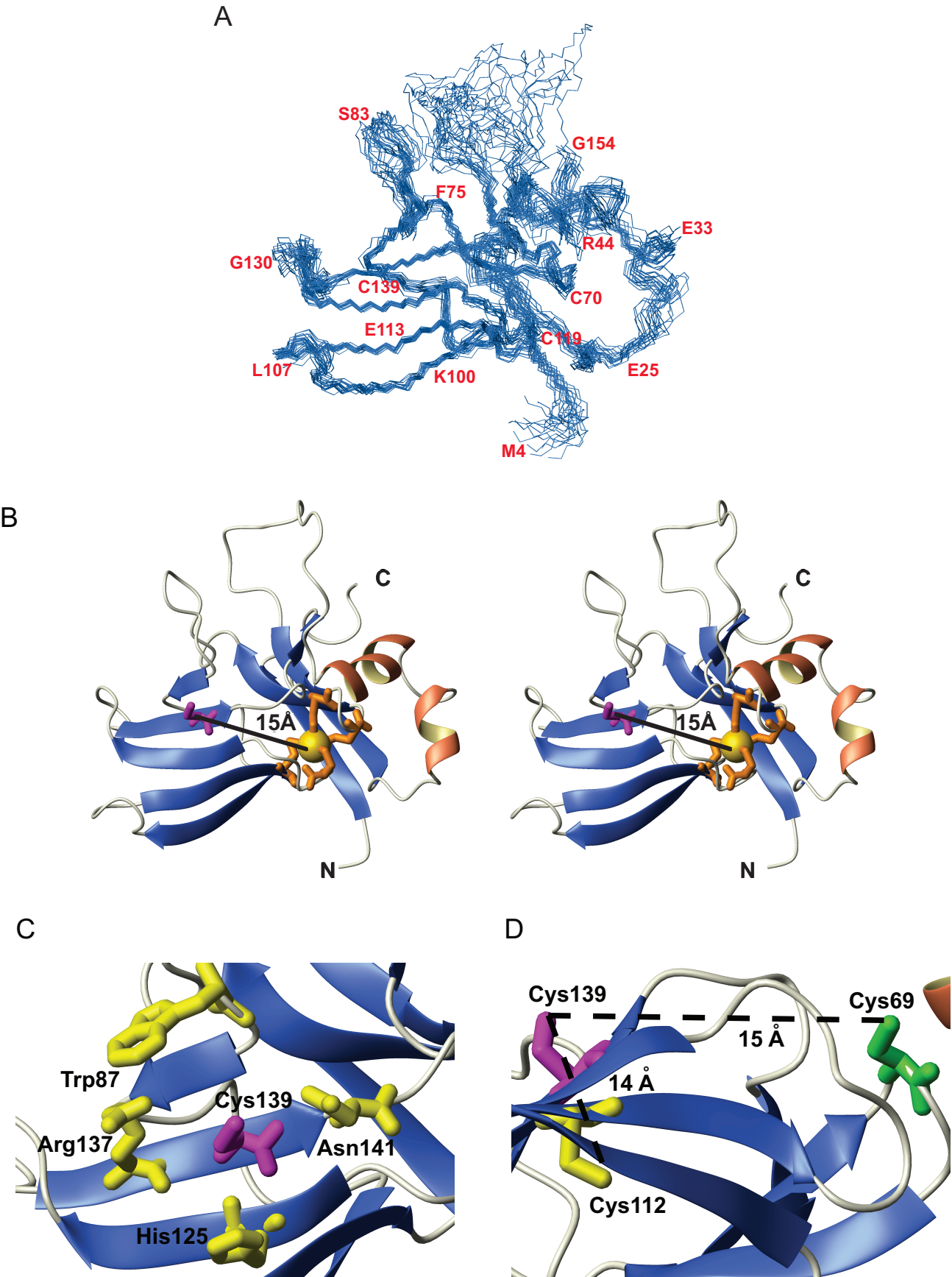

Figure 7

Carella, M et al. 2011
Molecular Microbiology
Accepted Manuscript Version

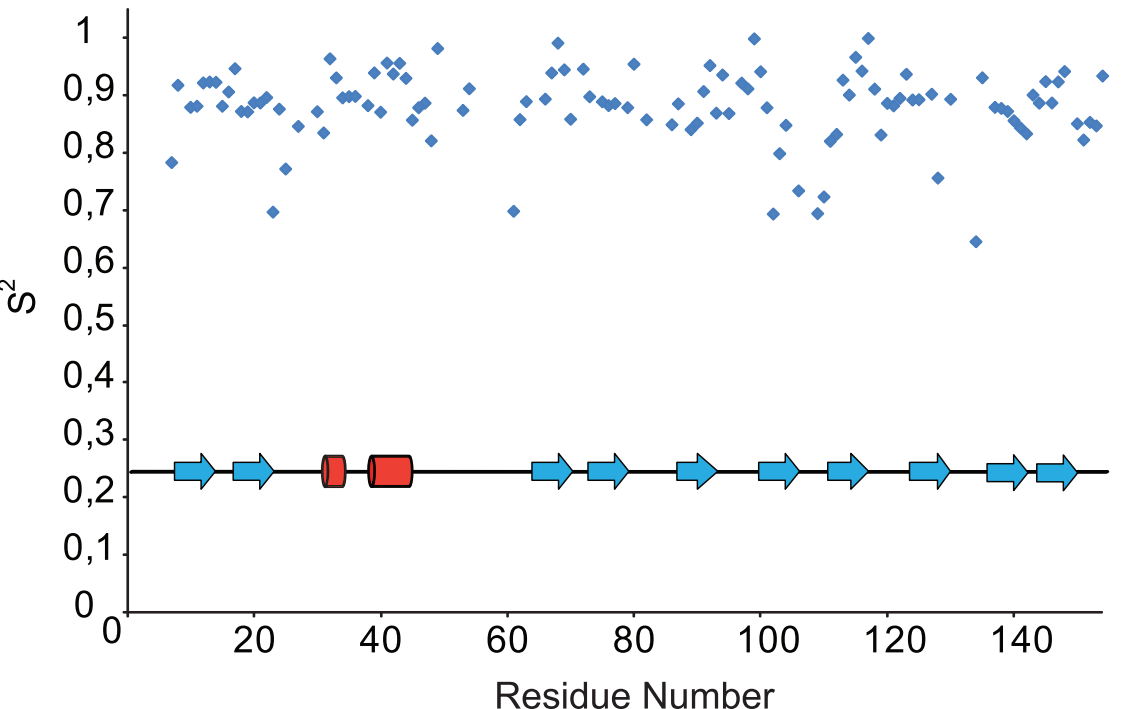

Figure 8

Carella, M et al. 2011
Molecular Microbiology
Accepted Manuscript Version

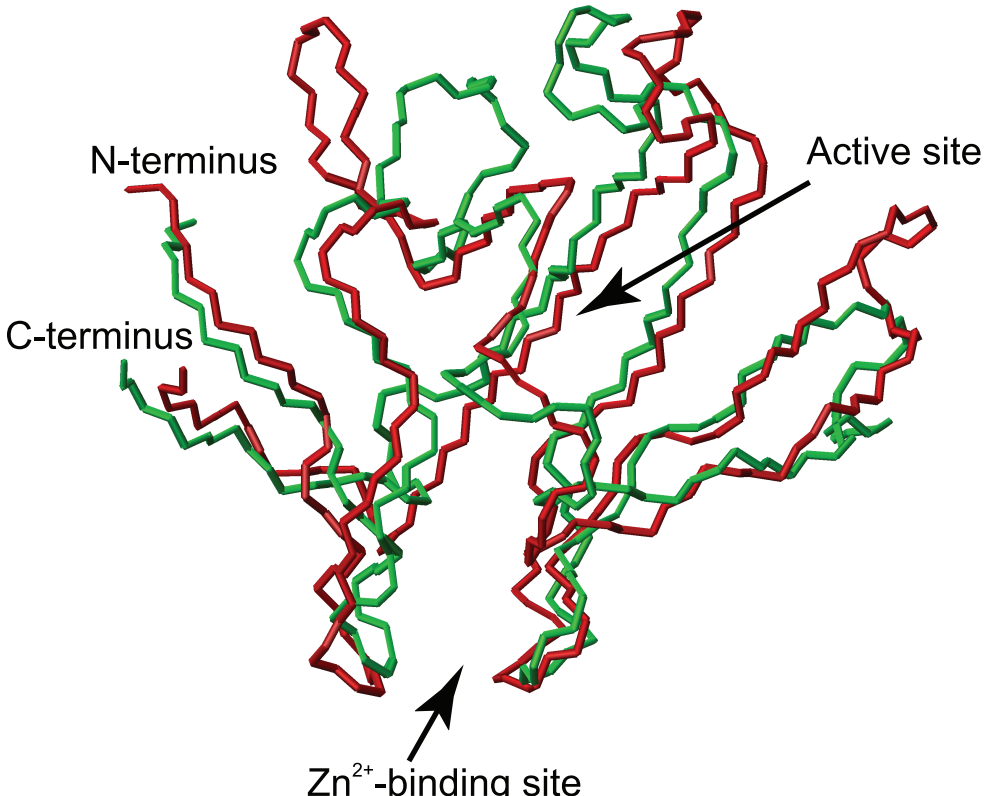

Figure 9

Carella, M et al. 2011
Molecular Microbiology
Accepted Manuscript Version

A

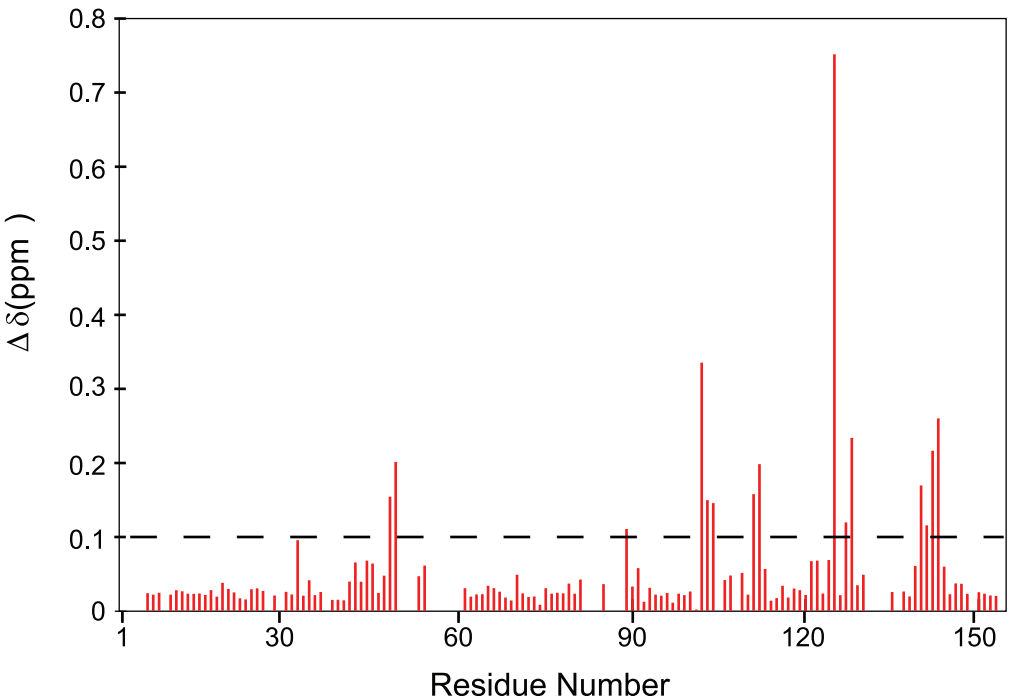

B

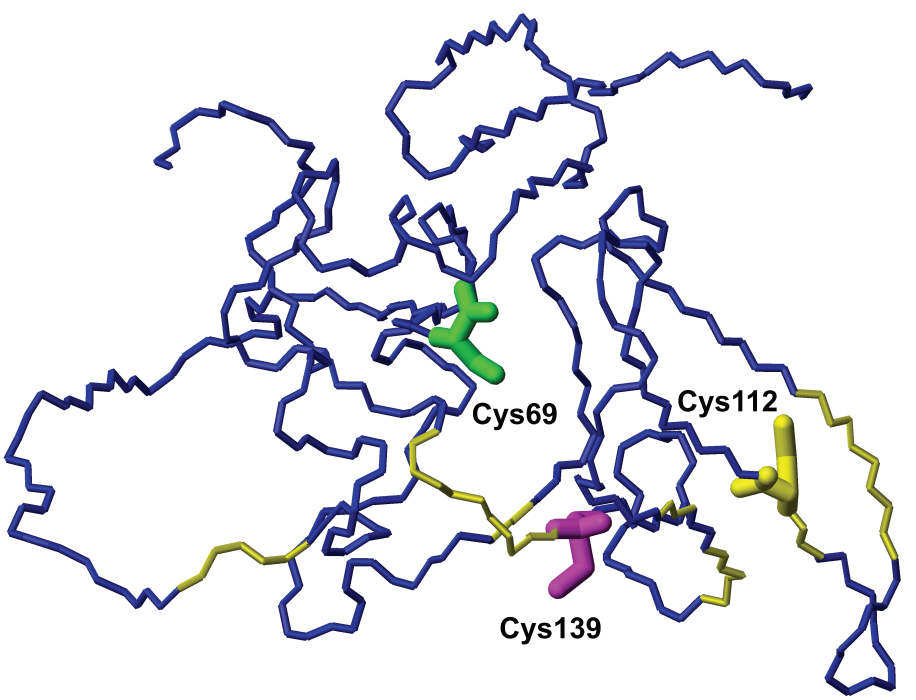

Carella, M et al. 2011
Molecular Microbiology
Accepted Manuscript Version

Structure–function relationship in an archaebacterial methionine sulfoxide reductase B

Supporting Information

Michela Carella, Juliane Becher, Oliver Ohlenschläger, Ramadurai Ramachandran, Karl-Heinz Gührs, Gerd Wellenreuther, Wolfram Meyer-Klaucke, Stefan H. Heinemann and Matthias Görlach

MTH711 activity on H_2O_2-oxidised calmodulin:

MTH711 activity was assayed using H_2O_2-oxidised calmodulin (CaM_{ox}) as substrate. CaM was overexpressed and purified as described previously (Roberts *et al.*, 1985). Protein concentration was measured using an ε_{280nm} of 2980 $M^{-1}cm^{-1}$. Methionines in CaM were oxidised upon incubation of 60 µM CaM (1 mg/mL) in 1.0 mM imidazole (pH 6.5), 10 mM $CaCl_2$ and 100 mM KCl with 100 mM H_2O_2 for 24 h at room temperature (Bartlett et al., 2003). The reaction was stopped by dialysing the sample against multiple changes of NMR buffer (20 mM Na-phosphate pH 7.2, 20 mM NaCl) (Bartlett et al., 2003). Oxidation was ascertained by MALDI-TOF mass spectrometry. 20 µM CaM was incubated with either 2 µM MTH711 or 2 µM human MSRA or with both enzymes in the presence of 10 mM DTT in 50 mM Tris/HCl pH 7.4 at 45 °C. Changes in the oxidation state of CaM were monitored by SDS-PAGE (Supporting Fig. 1) according to (Bartlett et al., 2003).

Supporting Figure 1

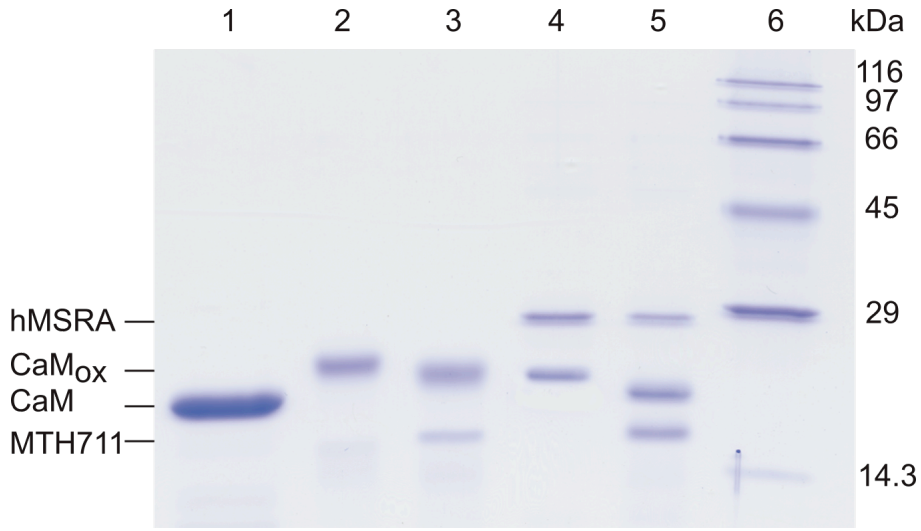

Supporting Figure 1. Reduction of H_2O_2 oxidised calmodulin by MTH711. SDS-PAGE (15% w/v polyacrylamide gel) showing the mobility changes of H_2O_2-oxidised calmodulin in the presence of MTH711 or human MSRA, both in the presence of 10 mM DTT. Lane 1: calmodulin (CaM); lane 2: oxidised calmodulin (CaM_{ox}); lane 3: CaM_{ox} following incubation with MTH711; lane 4: CaM_{ox} following incubation with hMSRA; lane 5: CaM_{ox} following incubation with MTH711 and hMSRA; lane 6: molecular weight markers; molecular weight indicated in kDa. The molecular species separated on the gel are indicated on the left.

This assay shows that oxidised CaM is partially reduced by either MSR: MTH711 (lane 3) or hMSRA (lane 4). Full reduction is achieved in the presence of both MSRs (lane 5).

References

Bartlett, R. K., R. J. Bieber Urbauer, A. Anbanandam, H. S. Smallwood, J. L. Urbauer & T. C. Squier, (2003) Oxidation of Met144 and Met145 in calmodulin blocks calmodulin dependent activation of the plasma membrane Ca-ATPase. *Biochemistry* **42**: 3231-3238.

Roberts, D. M., R. Crea, M. Malecha, G. Alvarado-Urbina, R. H. Chiarello & D. M. Watterson, (1985) Chemical synthesis and expression of a calmodulin gene designed for site-specific mutagenesis. *Biochemistry* **24**: 5090-5098.